

DEVELOPMENT AND VALIDATION OF TWO-PHASE FLOW MODELS AND CRITICAL HEAT FLUX PREDICTION FOR THE HIGHLY-SCALABLE CFD CODE NEK-2P

Nuclear Science and Engineering Division

About Argonne National Laboratory

Argonne is a U.S. Department of Energy laboratory managed by UChicago Argonne, LLC under contract DE-AC02-06CH11357. The Laboratory's main facility is outside Chicago, at 9700 South Cass Avenue, Argonne, Illinois 60439. For information about Argonne and its pioneering science and technology programs, see www.anl.gov.

DOCUMENT AVAILABILITY

Online Access: U.S. Department of Energy (DOE) reports produced after 1991 and a growing number of pre-1991 documents are available free via DOE's SciTech Connect (<http://www.osti.gov/scitech/>)

Reports not in digital format may be purchased by the public from the National Technical Information Service (NTIS):

U.S. Department of Commerce
National Technical Information Service
5301 Shawnee Rd
Alexandria, VA 22312
www.ntis.gov
Phone: (800) 553-NTIS (6847) or (703) 605-6000
Fax: (703) 605-6900
Email: **orders@ntis.gov**

Reports not in digital format are available to DOE and DOE contractors from the Office of Scientific and Technical Information (OSTI):

U.S. Department of Energy
Office of Scientific and Technical Information
P.O. Box 62
Oak Ridge, TN 37831-0062
www.osti.gov
Phone: (865) 576-8401
Fax: (865) 576-5728

Disclaimer

This report was prepared as an account of work sponsored by an agency of the United States Government. Neither the United States Government nor any agency thereof, nor UChicago Argonne, LLC, nor any of their employees or officers, makes any warranty, express or implied, or assumes any legal liability or responsibility for the accuracy, completeness, or usefulness of any information, apparatus, product, or process disclosed, or represents that its use would not infringe privately owned rights. Reference herein to any specific commercial product, process, or service by trade name, trademark, manufacturer, or otherwise, does not necessarily constitute or imply its endorsement, recommendation, or favoring by the United States Government or any agency thereof. The views and opinions of document authors expressed herein do not necessarily state or reflect those of the United States Government or any agency thereof, Argonne National Laboratory, or UChicago Argonne, LLC.

DEVELOPMENT AND VALIDATION OF TWO-PHASE FLOW MODELS AND CRITICAL HEAT FLUX PREDICTION FOR THE HIGHLY-SCALABLE CFD CODE NEK-2P

prepared by

Adrian Tentner, Prasad Vegendla, Dillon Shaver, Ananias Tomboulides, Aleks
Obabko, Elia Merzari

Nuclear Science and Engineering Division, Argonne National Laboratory

September 2018

SUMMARY

A project is underway to develop, verify and validate an advanced two-phase flow modeling capability for the highly-scalable high-performance CFD code NEK5000 [1]. The goal of the project is to develop a new two-phase version of the NEK5000 code, named NEK-2P, to simulate the two-phase flow and heat transfer phenomena that occur in a Boiling Water Reactor (BWR) fuel bundle under various operating conditions. The NEK-2P two-phase flow models follow the approach used for the Extended Boiling Framework [2-3] previously developed at Argonne, but include more fundamental physical models of boiling phenomena and advanced numerical algorithms for improved computational accuracy, robustness, and computational speed.

The development of the NEK-2P two-phase solver and the implementation of the Extended Boiling Framework two-phase models were supported by Argonne National Laboratory (Argonne) through an Laboratory Directed Research and Development (LDRD) project during FY14-16. The development and validation of the two-phase models through analyses of selected two-phase boiling flow experiments was supported by the Nuclear Energy Advanced Modeling and Simulation (NEAMS) program in FY17-18.

The report focuses on the extension of the NEK-2P Wall Heat Transfer model, which was initially developed for the analysis of Critical Heat Flux (CHF) under Dryout (DO) conditions to the simulation of CHF under Departure from Nucleate Boiling (DNB) conditions. The report presents results of recent NEK-2P analyses of several CHF experiments including both DO and DNB conditions. The CHF experiments analyzed have measured the axial distribution of wall temperatures in two-phase boiling flow in a vertical channel with a heated wall. The axial distribution of the calculated wall temperatures was compared with the corresponding experimental data. Reasonably good agreement with measured data was obtained in predicting the CHF location and post CHF wall temperature magnitudes illustrating the ability of the NEK-2P code and Advanced Boiling Framework (ABF) models to simulate the CHF phenomena for a wide range of thermal-hydraulic conditions. The onset of DNB location and the post DNB wall temperatures were in good agreement with experimental data using newly developed DNB models. In contrast, wall temperatures were underpredicted with the DO model. Furthermore, the newly developed DO-DNB model predicts reasonably well the measured wall temperatures for both DO and DNB experiments.

Apart from DO and DNB model development and validation, initial simulations are performed for Virginia Tech Air-water test loop. Also, a conjugate heat transfer model has been developed in NEK-2P. The simulations are underway for the Becker benchmark test using the conjugate heat transfer model.

Table of Contents

Summary	i
Table of Contents.....	ii
List of Figures.....	iii
List of Tables	iii
1 INTRODUCTION	1
2 TWO-PHASE MODELS OF THE NEK-2P CFD CODE	2
2.1 HOMOGENEOUS TWO-PHASE MODEL.....	2
2.2 DRIFT-FLUX TWO-PHASE MODEL	2
2.3 TWO-PHASE TWO-VELOCITY MODEL.....	2
2.3.1 The Two-Phase Two-Fluid Conservation Equations.....	3
2.4 THE ADVANCED BOILING FRAMEWORK	5
2.4.1 Inter-phase Surface Topology Map and Local Flow Configuration	6
2.4.2 Inter-phase mass, momentum, and energy transfer models	7
2.4.3 The wall-cell topology	7
2.5 CLADDING-TO-COOLANT HEAT TRANSFER MODEL	9
3 VALIDATION OF CHF DRYOUT EXPERIMENTS.....	12
3.1 CHF MODELING AND SIMULATIONS.....	12
3.1.1 Critical Heat Flux DO Experiments Analyzed.....	12
3.2 SIMULATION RESULTS AND DISCUSSION.....	14
3.3 CONCLUSIONS.....	20
4 VALIDATION OF CHF DNB EXPERIMENTS	21
4.1 SIMULATION OF TWO-PHASE BOILING FLOW IN CHF DNB EXPERIMENTS.....	21
4.2 CONCLUSIONS.....	29
5 PRELIMINARY SIMULATIONS WITH CONJUGATE HEAT TRANSFER MODEL.....	30
5.1 CONJUGATE HEAT TRANSFER MODEL	30
5.2 CONCLUSIONS.....	33
6 SIMULATIONS OF AIR-WATER EXPERIMENTS.....	34
6.1 NEK-2P AIR-WATER SIMULATIONS.....	34
6.2 CONCLUSIONS.....	36
7 STATUS OF THE TWO-FLUID TWO-PHASE MODEL	37
8 FUTURE WORK	37
ACKNOWLEDGMENTS	38
9 REFERENCES	39

LIST OF FIGURES

Figure 1. Schematic view of upward boiling flow in vertical channel with heated walls	5
Figure 2. Inter-phase Surface Topology Map used for the Advanced Boiling Framework.....	6
Figure 3. General four-field inter-phase surface topology.....	7
Figure 4. Wall cell general four-component topology and Heat Flux partition.....	8
Figure 5. Wall cell topology and Heat Flux partition for lower void fraction conditions	9
Figure 6. Schematic diagram of the Becker experiment [16]	13
Figure 7. Vapor volume fraction along XZ-plane; (a) Experiment A, (b) Experiment B, (c) Experiment C, (d) Experiment D, (e) Experiment E and (f) Experiment F.....	15
Figure 8. Wall temperature profiles along the tube height; (a) Experiment A, (b) Experiment B, (c) Experiment C, (d) Experiment D, (e) Experiment E and (f) Experiment F.....	18
Figure 9. Wall temperature along the tube height for experiment G	22
Figure 10. Contour fields for experiment G; (a) Vapor volume fraction, (b) Liquid temperature [K] and (c) Mixture velocity [m/s].....	23
Figure 11. Comparison of NEK-2P DO and DO-DNB models; (a) Wall temperature along the tube length and (b) Vapor volume fraction on a vertical plane (XZ- direction)	24
Figure 12. Wall temperature along the tube length for experiment H	25
Figure 13. Contour fields for experiment H; (a) Vapor volume fraction, (b) Liquid temperature [K] and (c) Mixture velocity [m/s].....	26
Figure 14. Wall temperature along the tube length for experiment I.....	27
Figure 15. Contour fields for experiment I; (a) Vapor volume fraction, (b) Liquid temperature [K] and (c) Mixture velocity [m/s].....	28
Figure 16. NEK-2P results along XZ-vertical slice for experiment A; (a) Vapor volume fraction and (b) Mixture velocity magnitude (m/s).....	31
Figure 17. NEK-2P results along XZ-vertical slice for experiment A; (a) Solid temperature [K] and (b) Liquid temperature [K].	32
Figure 18. Schematic diagram for Air-Water reactor [16].....	34
Figure 19. Air-water distribution at various axial locations for RUN-1 using $C_{lift}=0.02$	35
Figure 20. NEK-2P results along XZ-vertical slice of (a) Vapor volume fraction and (b) Mixture velocity magnitude (m/s).....	36

LIST OF TABLES

Table 1. Parameters of the CHF DO experiments analyzed	14
Table 2. Parameters of the CHF DNB experiment analyzed	14
Table 3. Operating conditions for VT experiments [16].....	35

1 INTRODUCTION

The NEK-2P two-phase CFD code is being developed at Argonne on the foundation of the high-fidelity highly-scalable CFD code Nek5000 [1] which provides general high-fidelity single-phase flow modeling capabilities. NEK-2P is designed to simulate the two-phase flow and heat transfer phenomena that occur in Light Water Reactor (LWR) fuel bundles under various operating conditions. The NEK-2P two-phase flow models utilize the Extended Boiling Framework [2] methodology previously developed at Argonne, which has been extended to include more fundamental physical models of boiling flow and heat transfer phenomena and advanced numerical algorithms for improved computational accuracy and computational speed. Previous work including the initial implementation of the Extended Boiling Framework (EBF) in the CFD code STAR-CD showed promising potential for the fine-mesh, detailed simulation of fuel assembly two-phase flow phenomena [3, 4], including the occurrence of Critical Heat Flux (CHF) [5].

The present work focuses on the development, and validation of the NEK-2P two-fluid two-phase model (2F-2P), including the extension of the Wall Heat Transfer model and CHF prediction under conditions of interest for LWRs. The report reviews the EBF and Advanced Boiling Framework (ABF) models and presents results of recent NEK-2P analyses of several CHF experiments that have measured the axial distribution of the wall temperature in two-phase upward flow in a vertical channel with a heated wall. These analyses include both CHF experiments under DO and DNB conditions which supplement the CHF DO results presented in [6]. The simulated axial distribution of the wall temperature is compared with experimental data. Good agreement with measured data is observed in predicting the dryout location and post dryout wall temperature magnitudes, illustrating the ability of the NEK-2P code and ABF models to simulate the CHF phenomena for a wide range of thermal-hydraulic conditions including DNB. The report concludes with a discussion of results and plans for future work.

2 TWO-PHASE MODELS OF THE NEK-2P CFD CODE

The development of the NEK-2P has followed a staged approach, beginning with the development of a homogeneous two-phase model in FY 2014, continuing with the development of a more complex two-phase drift-flux model in FY 2015, and followed with the implementation of a two-phase two-velocity model for NEK-2P in FY 2016 and FY 2017. In FY18 additional features were developed in NEK-2P such as the Departure from Nucleate Boiling (DNB) CHF model and the Conjugate Heat Transfer model. The initial implementation of these two-phase models has been completed and their formulation and assumptions are described below.

2.1 HOMOGENEOUS TWO-PHASE MODEL

Because only one velocity field is available in the Low-Mach version of NEK5000, we decided to begin with the implementation of a homogeneous two-phase model. The main assumptions of the homogeneous model are: i) the local velocities of the water and vapor phases are assumed to be the same for each computational element, and ii) the local temperatures of the water and vapor phases are assumed to be the same for each computational node. The phase transition from water to vapor is due to local enthalpy changes in a reactor fuel assembly or in a heated pipe experiment are driven by the wall heat flux. The mass, momentum, and energy conservation equations can be found in Tentner et al. [7].

2.2 DRIFT-FLUX TWO-PHASE MODEL

The development of the drift-flux model is an intermediate step in the development of the two-phase NEK-2P code. The approach selected by the development team is intended to extend the capabilities of the homogeneous two-phase model described above in a manner that minimizes the changes to the one-velocity two-phase solver and to provide a test-bed for the implementation of the Extended Boiling Framework while the two-velocity two-phase solver of the NEK-2P code is being developed.

The drift-flux model accounts for the effect of different vapor and liquid velocities within the framework of the one-velocity solver. The current model allows different phase velocities, but assumes that the liquid and vapor have the same temperature in each computational cell. The calculation of the local liquid and vapor velocities requires the use of the Extended Boiling Framework as described in Tentner et al. [7].

2.3 TWO-PHASE TWO-VELOCITY MODEL

The NEK-2P two-velocity two-phase model development includes two sets of transport equations for mass, momentum, and energy for water and vapor phases. The full details of the transport equations and associated closures of Extended Boiling Framework (EBF) can be found in Tentner et al. [5]. Currently, the validation is underway for two-velocity two-phase model in NEK-2P code for both critical heat flux and subcooled boiling flow benchmark tests [8].

Nek5000 [1] is a highly-scalable open-source transient CFD code developed at Argonne National Laboratory which has been awarded the Gordon Bell prize in high-performance computing and has run on over one million processors on Argonne's massively parallel Blue Gene/Q computer Mira. The code is based on the spectral element method and it is written in FORTRAN 77 and C languages. The original Nek5000 was built for the simulation of single phase constant-density flows. A later version of the code, referred to as the Low-Mach version, was modified to allow the simulation of single-phase variable-density perfect-gas flows. The Low-Mach version of Nek5000 was selected by the project team as the platform for the implementation of two-phase boiling modeling capabilities in NEK-2P. The development of NEK-2P has followed a staged approach, beginning with the development of a homogeneous two-phase model and continuing with a more complex two-phase drift-flux model. The implementation of these two-phase models was described in Tentner et al. [7]. The development of a two-phase two-fluid solver for NEK-2P and the coupling of this solver with the EBF models have later been completed. The 2P-2F solver and the associated models which are used in the CHF experiment analyses presented in this report are reviewed below.

2.3.1 The Two-Phase Two-Fluid Conservation Equations

A new two-phase two-fluid solver has been implemented in NEK-2P, replacing the previous Nek5000 solver which could only track one fluid velocity field. The new NEK-2P Eulerian two-phase two-fluid solver calculates time evolution of the mass, velocity, and energy of the liquid and vapor phases at all mesh locations in the computational domain by solving the mass, momentum and energy conservation equations for each phase.

The conservation of mass equation for phase k is:

$$\frac{\partial}{\partial t}(\alpha_k \rho_k) + \nabla \cdot (\alpha_k \rho_k \mathbf{u}_k) = \dot{m}_{ki} - \dot{m}_{ik} \quad (1)$$

The conservation of momentum equation for phase k is:

$$\begin{aligned} \frac{\partial}{\partial t}(\alpha_k \rho_k \mathbf{u}_k) + \nabla \cdot (\alpha_k \rho_k \mathbf{u}_k \mathbf{u}_k) - \nabla \cdot (\alpha_k (\boldsymbol{\tau}_k + \boldsymbol{\tau}_k^t)) = \\ - \alpha_k \nabla P + \alpha_k \rho_k \mathbf{g} + \mathbf{M} \end{aligned} \quad (2)$$

The conservation of energy equation for phase k is:

$$\frac{\partial}{\partial t}(\alpha_k \rho_k e_k) + \nabla \cdot (\alpha_k \rho_k \mathbf{u}_k e_k) - \nabla \cdot (\alpha_k \lambda_k \nabla T_k) = Q \quad (3)$$

The momentum equations for the two phases are currently coupled through the pressure, which is assumed to be the same for the two phases. The mass, momentum, and energy phase conservation equations are also coupled through the corresponding inter-phase transfer terms, which are obtained using the Extended Boiling Framework (EBF) models.

The inter-phase forces considered in the model are: drag, turbulent dispersion, virtual mass, lift, and wall lubrication forces. In addition, inter-phase momentum transfer is associated with mass transfer hence \mathbf{M} in Equation 2 is given by:

$$\mathbf{M} = \mathbf{F}_D + \mathbf{F}_T + \mathbf{F}_M + \mathbf{F}_L + \mathbf{F}_{WL} + \dot{m}_{ki} \mathbf{u}_i - \dot{m}_{ik} \mathbf{u}_k \quad (4)$$

The treatment of the inter-phase forces covers the spectrum of flow topologies expected in a BWR fuel assembly. The drag force model, for example, covers bubbles in the sub-cooled or saturated bubbly flow topology, a mixture of Taylor bubbles and smaller bubbles in the slug-flow transition topology, and droplets in the droplet or mist topology. Details of the treatment of inter-phase forces can be found in Tentner et al. [8] and Ustinenko et al. [4]. The inter-phase heat transfer term Q in Equation 3 is obtained by considering the heat transfer from the vapor and the liquid to the gas/liquid interface assumed to be at the saturation temperature, as described in Tentner et al. [9].

The turbulence effects are currently included through an algebraic mixing-length model. An extended $k - \omega$ model that contains extra source terms that arise from the inter-phase forces present in the momentum equations is under development.

The solution of two-fluid two-phase model (2F-2P) equations implemented in NEK-2P is based on a novel low-Mach-number numerical approach, based on previous work on reactive gaseous flow [10-11]. In this approach, the pressure is assumed to be the same for both phases. The solution method was described in detail in Tentner et al. [6].

The required phenomenological closures for the continuity, momentum and the energy equations were taken from the Extended Boiling Framework (EBF) work of Tentner et al. [2]. The Advanced Boiling Framework (ABF) included in the NEK-2P code uses a four-field two-phase generalized topology representation - described below in Section 2.4 - for a more accurate prediction of interfacial area and associated mass, momentum, and energy inter-phase transfer.

2.4 THE ADVANCED BOILING FRAMEWORK

Inter-phase interactions in multiphase fluids depend on both the area and the topology of the phase interface. Sub-channel thermal-hydraulic codes rely on flow regime maps to evaluate the interface topology using cross-section-averaged flow parameters. CFD codes, which divide the flow space into much finer computational cells cannot rely on the traditional sub-channel flow regimes, but must evaluate instead the local topology. The ensemble of many computational cells with relatively simple topologies can provide complex global two-phase flow topologies that include all the traditional sub-channel flow regimes. The definition of the local inter-phase surface topology and the subsequent calculation of the mass, momentum, and energy inter-phase interactions is based on the use of the Extended Boiling Framework [2, 9] which has been implemented in NEK-2P and is reviewed in this section. Flow topology changes typical for boiling flow in BWR fuel assemblies and the local topologies considered in the EBF are illustrated schematically in Figure 1.

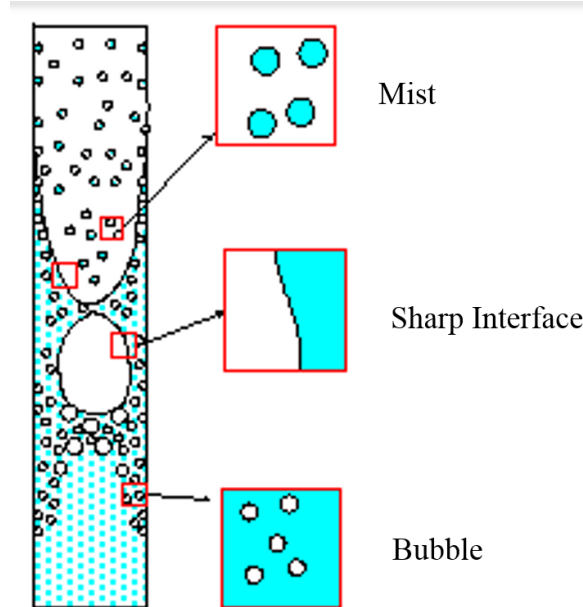


Figure 1. Schematic view of upward boiling flow in vertical channel with heated walls

While the initial EBF models were based on a two-field representation of the local topology, the NEK-2P implementation of the EBF has been extended to include a more general four-field representation of the local topology which allows a more rigorous treatment of the inter-phase interaction terms and is referred to as the Advanced Boiling Framework (ABF). A brief discussion of the new ABF features is included below. The ABF models are integrated with the new two-phase two-fluid solver.

2.4.1 Inter-phase Surface Topology Map and Local Flow Configuration

The EBF boiling model uses a locally calculated topology variable to allow the following topologies: a) a bubbly flow topology with spherical vapor bubbles in a continuous liquid, b) a droplet or mist topology with spherical liquid droplets flowing in a continuous vapor field, and c) a transition topology which combines the features of the two previous topologies in various proportions. The local topology is determined in this model using a local topology map based on the local void fraction. The 1-dimensional topology map used for cells that are not adjacent to solid walls is illustrated in Figure 2 together with the associated local flow topologies. The topology variable which assumes values between 0-1 is based on the local vapor volume fraction and is then used in the code to determine the local topology and calculate the corresponding mass, momentum, and energy inter-phase transfer terms.

While the original Extended Boiling Framework (EBF) relies on a two-field representation of the local topology (liquid and vapor), the Advanced Boiling Framework recently implemented in NEK-2P introduces a more general four-field representation of the local inter-phase surface topology, illustrated in Figure 3.

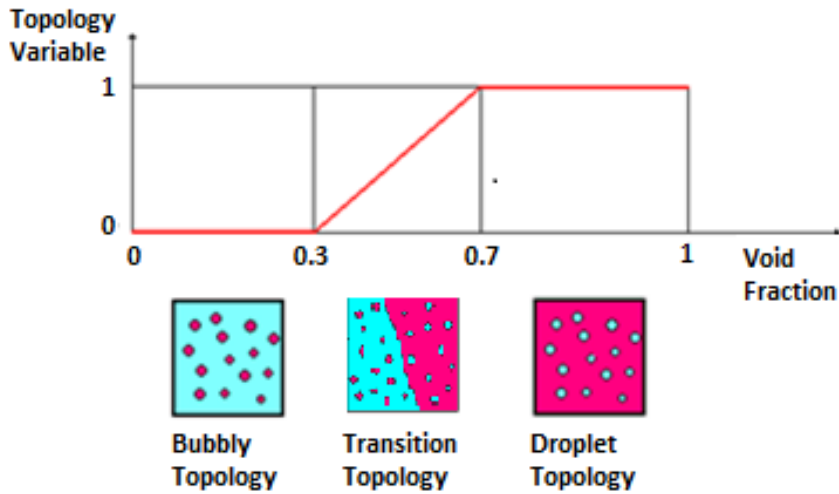


Figure 2. Inter-phase Surface Topology Map used for the Advanced Boiling Framework

The general four-field topology provides the foundation for the definition of local topologies in all the computational cells, but affects directly the topology in the interior transition cells and in the wall cells. In the interior cells with bubbly or droplet flow regimes only two fields are used (see Figure 2) and the ABF cell topology remains the same as the two-field EBF topology. In the interior transition topology cells and in the wall cells the use of the four-field ABF topology instead of the two-field EBF topology allows a more detailed treatment of the relevant two-phase flow phenomena. The use of the four-field ABF topology in the wall cells is described in the following sections.

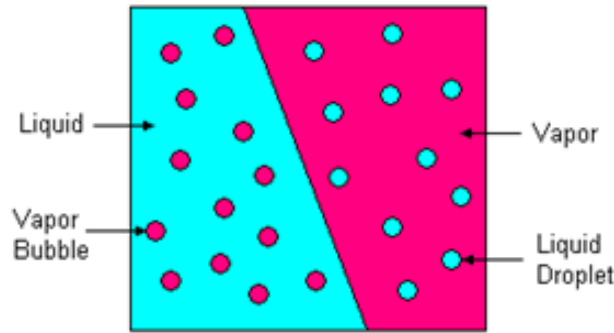


Figure 3. General four-field inter-phase surface topology

2.4.2 Inter-phase mass, momentum, and energy transfer models

The inter-phase surface topology map is used to evaluate the interfacial area and inter-phase interactions. Three basic local flow configurations with specific interface topology are identified (bubbly flow, mist flow and sharp interface) and the interfacial area and inter-phase mass, momentum, and energy transfer models are defined for these configurations. In the domain identified in Figure 2 as transitional topology it is assumed that a combination of basic flow configurations is present, separated by a phase interface with geometric characteristics typical of larger Taylor bubbles. Both small bubbles with a prescribed diameter and large Taylor bubbles are considered in the transition-topology cells. The diameter of the Taylor bubbles is assumed comparable to the channel hydraulic diameter. The quantities required for closure are found by determining the appropriate combination of mass, momentum, and energy exchange terms for the local flow topology. The most general transitional topology is illustrated in Figure 3, and various other transitional topologies are obtained by retaining only a sub-set of the transition master-cell features.

As demonstrated in [12], the use of the local inter-phase surface topology map allows the modeling of complex sub-channel-scale topologies that emerge from combinations of many computational cells with one of the local topologies shown in Figure 2. E.g., the typical sub-channel annular flow regime illustrated in Figure 1 could be resolved into a distinct core flow region in which the gas phase is continuous and the local mist topology is used, separated by transition topology cells from a liquid film on the wall where the local bubbly topology and the wall-cell topology are used.

2.4.3 The wall-cell topology

The wall cell topology is a special case of the general cell topology discussed above. Wall cells where the local liquid volume fraction is lower than a specified value are treated in the ABF boiling model as a special liquid film and droplet topology illustrated in Figure 4. The wall cells can contain both a liquid film and liquid droplets. As the liquid volume fraction decreases the liquid film, which initially covers the entire wall surface is assumed to become unstable and to cover the wall surface only partially. This wall cell topology is representative for conditions that can lead to the occurrence of CHF under Dryout (DO) conditions.

Because the 2F-2P solver allows only one velocity and one temperature for each phase in a computational cell, the droplet and film velocities and temperatures are the same. However, the partition of the liquid between the liquid film and droplets has important implications for the heat transfer between the heated wall and the two-phase coolant. The explicit partition of liquid between the film and droplets in the wall cells allows a more detailed partition of the wall heat flux allowing an improved prediction of the CHF under DO conditions.

The CHF can occur under Departure from Nucleate Boiling (DNB) conditions at lower local void fractions due to high wall heat flux values. In this case the wall cell topology is simplified, with the liquid covering the entire wall area. The CHF can still occur due to the increasing number of departing vapor bubbles, which prevent or delay the re-wetting of the heated wall by the liquid, as illustrated in Figure 5.

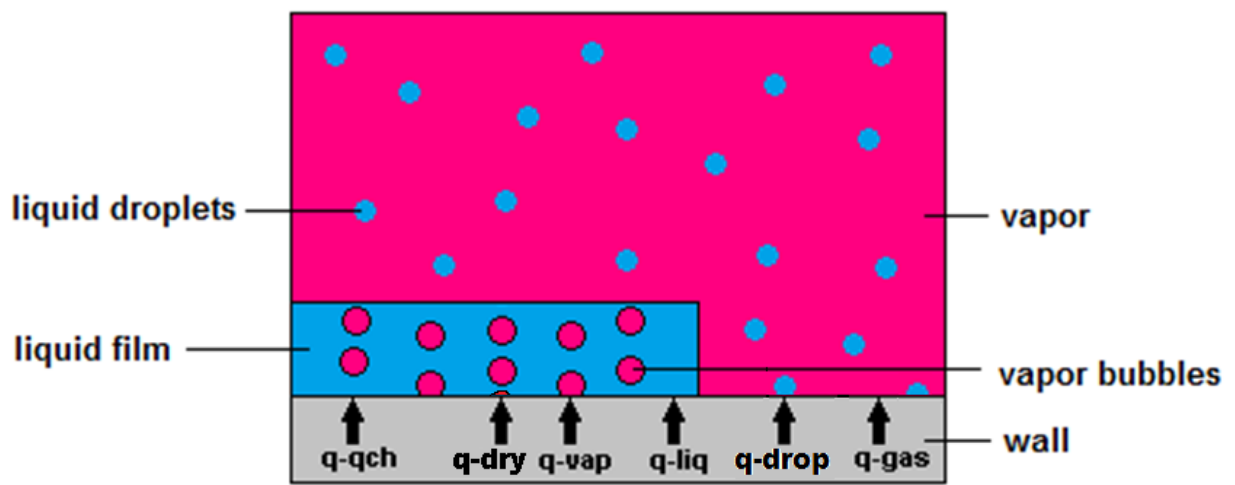


Figure 4. Wall cell general four-component topology and Heat Flux partition

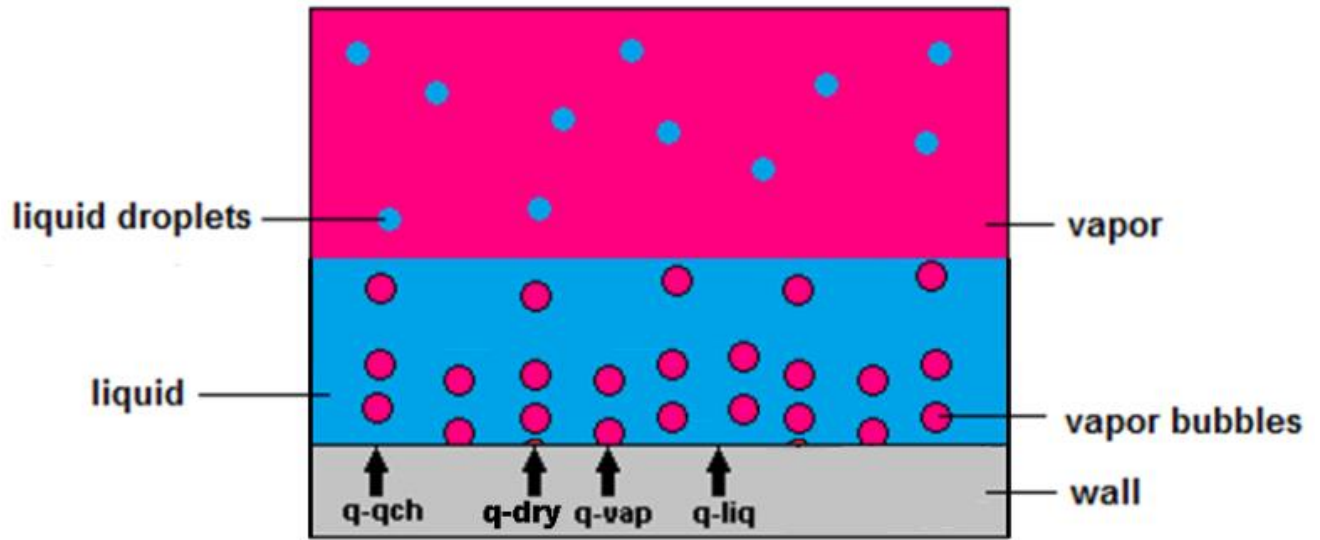


Figure 5. Wall cell topology and Heat Flux partition for lower void fraction conditions

2.5 CLADDING-TO-COOLANT HEAT TRANSFER MODEL

The calculation of the wall temperature and CHF prediction is based on partitioning of heat flux between six heat transfer components as illustrated in Figure 4. The new six-component heat flux partition replaces the previous five component partition presented in [6] and is designed to improve the modeling of the wall heat transfer phenomena which influence the CHF occurrence.

The wall heat flux is partitioned between the following six heat transfer components illustrated in Figure 4: a) q_{gas} , the convective heat flux from wall to the gas or vapor phase, over the wall area not covered by the liquid film; b) q_{drop} , the convective heat flux from wall to the liquid droplets, over the wall area not covered by the liquid film; c) q_{liq} , the convective heat flux from wall to the liquid phase, over the area covered by the liquid film but excluding the bubble nucleation area; d) q_{vap} , the evaporation heat flux from wall to the boiling interface, over the bubble nucleation area, during the bubble growth phase of the bubble formation and departure cycle e) q_q , the quenching heat flux from the wall to the liquid over the nucleation area, during the quenching phase of the bubble formation and departure cycle, and f) q_{dry} , the heat flux from the wall to the vapor over the nucleation area during the dry-wall phase which is assumed to follow the bubble departure and to precede the quenching phase. These heat flux components are specified per unit wall area and they decrease or become zero as the corresponding wall-contact area decreases. The wall heat flux is given by:

$$q_w = q_{gas} + q_{drop} + q_{liq} + q_{vap} + q_{qch} + q_{dry} \quad (5)$$

The heat flux components are calculated using the appropriate heat transfer coefficients and heat transfer area based on the local wall-cell topology:

$$q_{gas} = h_g \theta_{dry} (1 - \theta_{drop}) (T_w - T_g) \quad (6)$$

$$q_{drop} = h_d \theta_{dry} \theta_{drop} (T_w - T_l) \quad (7)$$

$$q_{liq} = h_l (1 - \theta_{dry}) (1 - \theta_{bn}) (T_w - T_l) \quad (8)$$

$$q_{vap} = h_l (1 - \theta_{dry}) \theta_{bn} f_{vap} (T_w - T_{sat}) \quad (9)$$

$$q_{qch} = h_q (1 - \theta_{dry}) \theta_{bn} f_{qch} (T_w - T_l) \quad (10)$$

$$q_{dry} = h_g (1 - \theta_{dry}) \theta_{bn} f_{dry} (T_w - T_l) \quad (11)$$

where θ_{dry} is the fraction of the total cell wall area covered by vapor, θ_{drop} is the fraction of the dry wall in contact with the liquid droplets, θ_{bn} is the fraction of the area covered by liquid which is covered by bubble nucleation sites, and f_{vap} , f_{qch} , f_{dry} are the fractions of the bubble formation and departure time cycle represented by the respective cycle phases shown in Eq. 12.

The formulation of the previous wall heat transfer model based on partitioning the heat flux into five components (q_{gas} , q_{liq} , q_{vap} , q_{qch} , q_{drop}) was described in [6]. This model is referred below as the CHF DO model. The sixth component of the wall heat flux q_{dry} represents the heat transferred between the heated wall and the bubble nucleation sites during the dry-out period assumed to follow the bubble departure from the wall. It has been added in order to better represent the phenomena that affect the CHF under DNB conditions. The six-component heat flux partitioning model is referred below as the CHF DO-DNB model. In the CHF DO model the bubble formation and departure cycle is divided into two phases, the bubble growth and the quenching phase, following the Kurul-Podowski model [13]. In the new CHF DO-DNB model the bubble formation and departure cycle is divided into three phases: the bubble growth phase, the dry-out phase that follows the bubble departure, and the quenching phase.

$$t_{BB}^{cycle} = t_{vap} + t_{dry} + t_{qch} \quad (12)$$

The length of the dry-out period t_{dry} is a function of the wall superheat and under DO conditions is equal to zero or remains small, so that the six-component heat partitioning model becomes equivalent to the five-component CHF DO model. Under DNB conditions however t_{dry} becomes significant and plays an important role in the prediction of CHF DNB as illustrated in Chapter 4. The length of the dry-out period t_{dry} is based on the value of the nucleation site density obtained from [2, 13]:

$$n'' = (m \Delta T_{sup})^p \quad (13)$$

where $\Delta T_{sup} = T_{wall} - T_{sat}$ is the wall superheat, $m=185$ and $p=1.805$ [13]. As long as the wall area occupied by the bubbles does not exceed the total liquid film area Equation 13 is used and $t_{dry}=0$. If the wall superheat ΔT_{sup} exceeds ΔT_{dry} when the wall area occupied by the bubbles exceeds the total liquid film area the nucleation site density cannot increase anymore and instead t_{dry} increases as a function of $(\Delta T_{sup} - \Delta T_{dry})$:

$$t_{dry} = t_{BB,o}^{cycle} C(\delta_{film}) \left(\frac{\Delta T_{sup}}{\Delta T_{dry}} - 1 \right) \quad (14)$$

Where $t_{BB,o}^{cycle}$ is the length of the bubble-cycle before the occurrence of dry-out and $C(\delta_{film})$ is a coefficient that accounts for the effect of the liquid film thickness. The wall-cell topology illustrated in Figure 4 and the heat flux partitioning models described above are used the analysis of the CHF experiments described in Chapter 3.

3 VALIDATION OF CHF DRYOUT EXPERIMENTS

3.1 CHF MODELING AND SIMULATIONS

In this study, a set of six Critical Heat Flux (CHF) benchmark tests performed under DO conditions were analysed in order to validate NEK-2P two-phase two-fluid (2P-2F) solver and the ABF two-phase closure models for a range of mass flow rates and wall-heat fluxes. Three of these benchmarks were presented in [6, 14] and are also described below. Three more boiling flow CHF experiments performed under DO conditions were analysed recently and published in ICONE26 [14].

3.1.1 Critical Heat Flux DO Experiments Analyzed

A schematic of the experimental test section is presented in Figure 6. The experiment was conducted in a vertical channel 0.01 m in diameter and 7 m in length with a uniformly heated wall. The outer wall temperature was measured with 55 Chromel-Alumel thermocouples placed along the heated length of the pipe. Between inlet and 3.00 m the thermocouples were installed at 0.25 m intervals, while between 3.00 m and outlet the interval between thermocouples was 0.1 m. The inner wall temperatures were obtained from the outer wall temperatures through integration of the heat transfer equation. The accuracy of the thermocouples is not reported in Becker et al. [15] but a review of the literature shows that the accuracy of Chromel-Alumel thermocouples has remained ~2.2 C or 0.75% for many years both before and after the experiment. The outlet pressure was approximately 7 MPa and the inlet sub-cooling was approximately 10.3 K. The experiments differed in inlet mass flux G and wall heat flux q_w as shown in Table 1 and Table 2, which also include the ratio q_w/G for each experiment. Table 1 contains the parameters of the six CHF DO experiments analysed to-date, with the recently analysed experiments A, B, and F highlighted. Only a very small number of experiments where CHF occurred under DNB conditions were identified. We analysed experiments G, H and I, with parameters listed in Table 2 in Chapter 4.

A schematic of the experimental test section is presented in Figure 6. The experiment was conducted in a vertical channel 0.01 m in diameter and 7 m in length with a uniformly heated wall. The pressure was approximately 7 MPa and the inlet sub-cooling was approximately 10.3 K. The experiments differed in inlet mass flux G and wall heat flux q_w as shown in Table 1, which also includes the ratio q_w/G for each experiment.

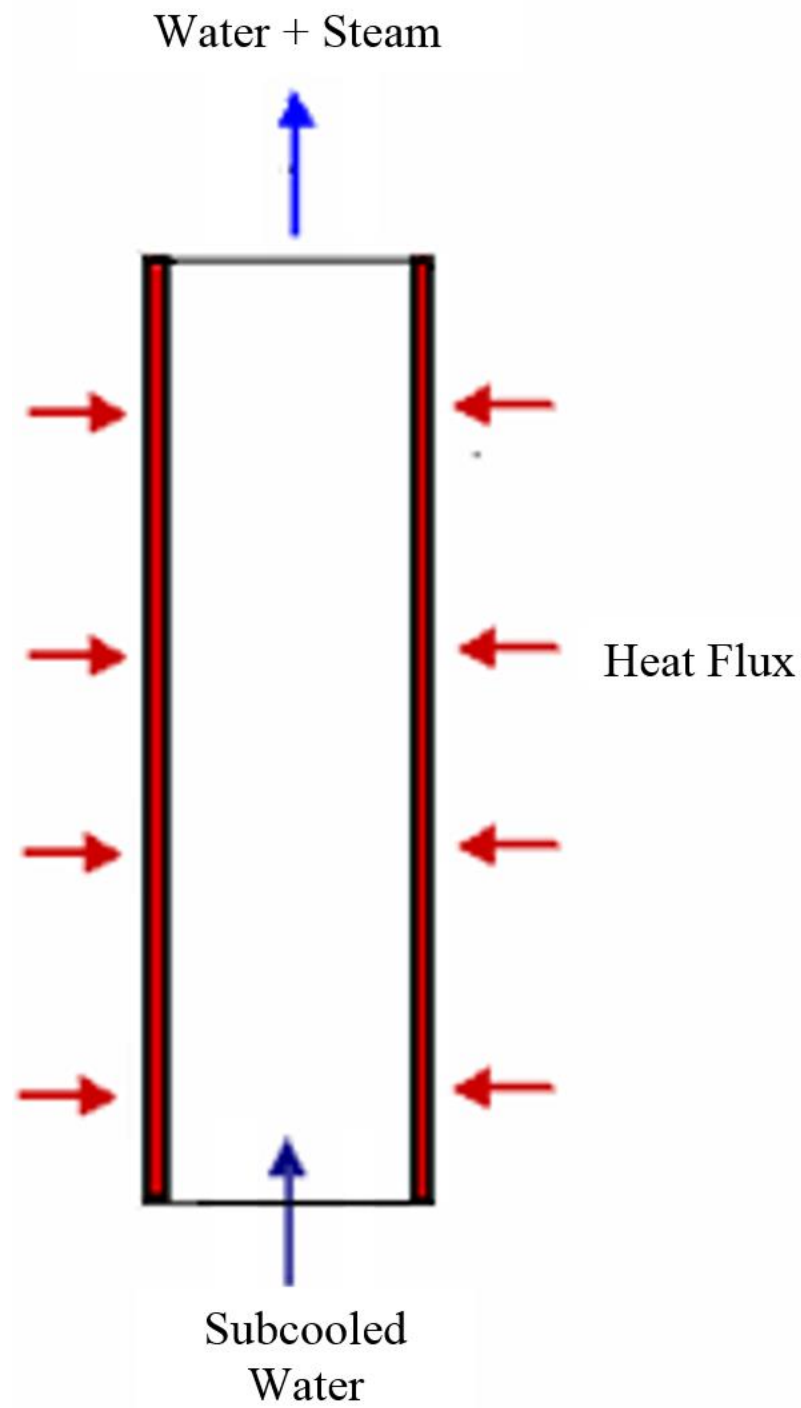


Figure 6. Schematic diagram of the Becker experiment [15]

Table 1. Parameters of the CHF DO experiments analyzed

Exp.	G [kg/s-m ²]	q_w [W/m ²]	$T_{in}-T_{sat}$ [K]	q_w/G [J/kg]	Pressure [bar]
A	497.0	35.0e4	-10.3	704	70
B	1009.6	40.1e4	-10.3	397	70
C	1008.9	49.9E4	-10.3	495	70
D	1495.0	79.7E4	-10.3	533	70
E	1994.9	79.6E4	-10.3	399	70
F	2482.9	80.0e4	-10.3	322	70

Table 2. Parameters of the CHF DNB experiment analyzed

Exp.	G [kg/s-m ²]	q_w [W/m ²]]	$T_{in}-T_{sat}$ [K]	q_w/G [J/kg]	Pressure [bar]
G	1507.4	59.8e4	-10	396	200
H	1013.1	39.6e4	-10	390	200
I	1017	29.7	-10	292	200

3.2 SIMULATION RESULTS AND DISCUSSION

The calculated void fraction distributions for the three experiments analyzed are shown in Figures 7a through 7f. The characteristic sub-channel flow regimes in a pipe with heated walls are simulated. Since the inlet temperature was only 10.3 K below saturation the bubbly flow regime is limited to the near-inlet region of the pipe. The annular-mist flow regime with annular liquid films on pipe wall and the mist flow regime are clearly observed in all three numerical simulations. The calculated wall temperature as a function of the distance from the pipe inlet is shown in Figures 8a through 8f.

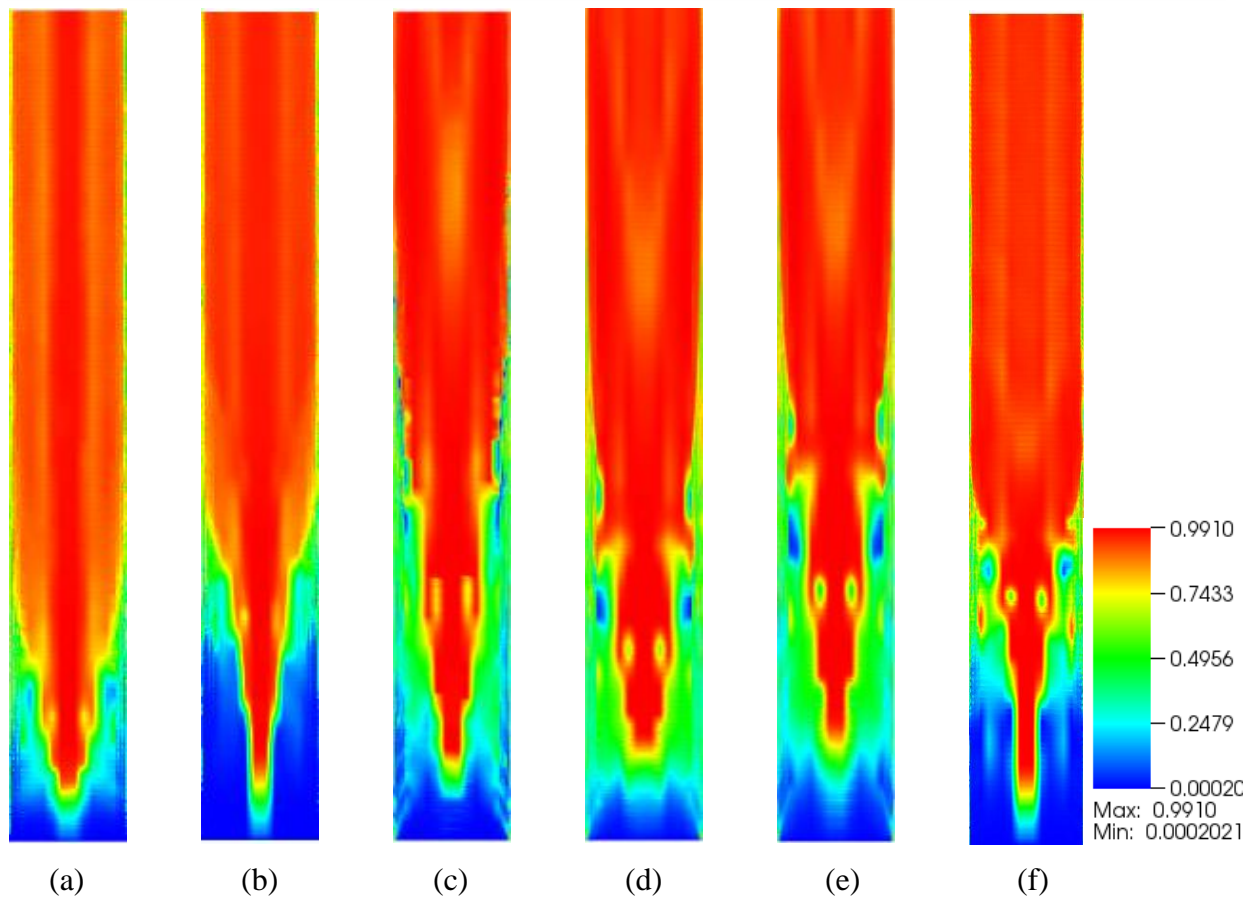
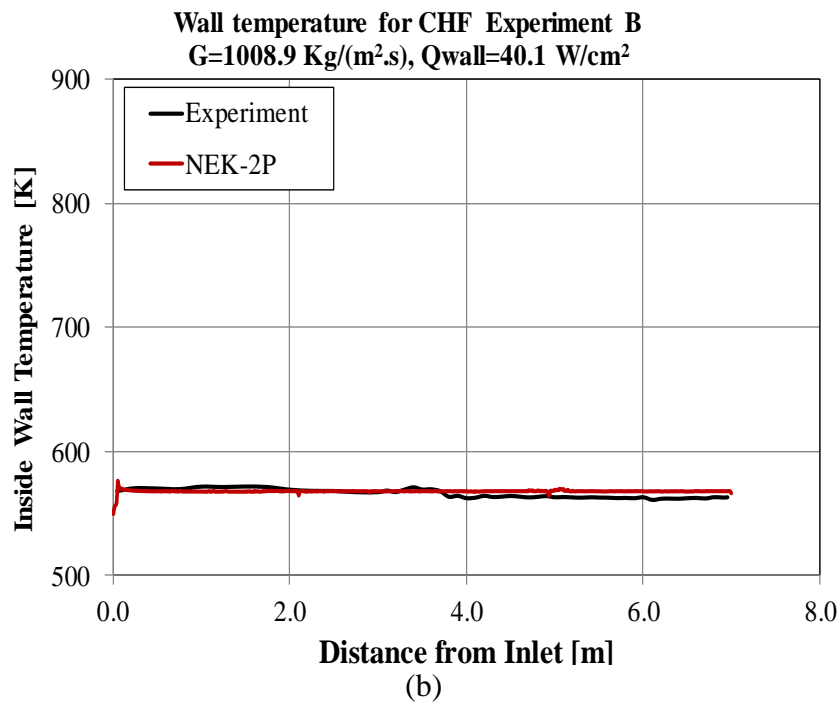
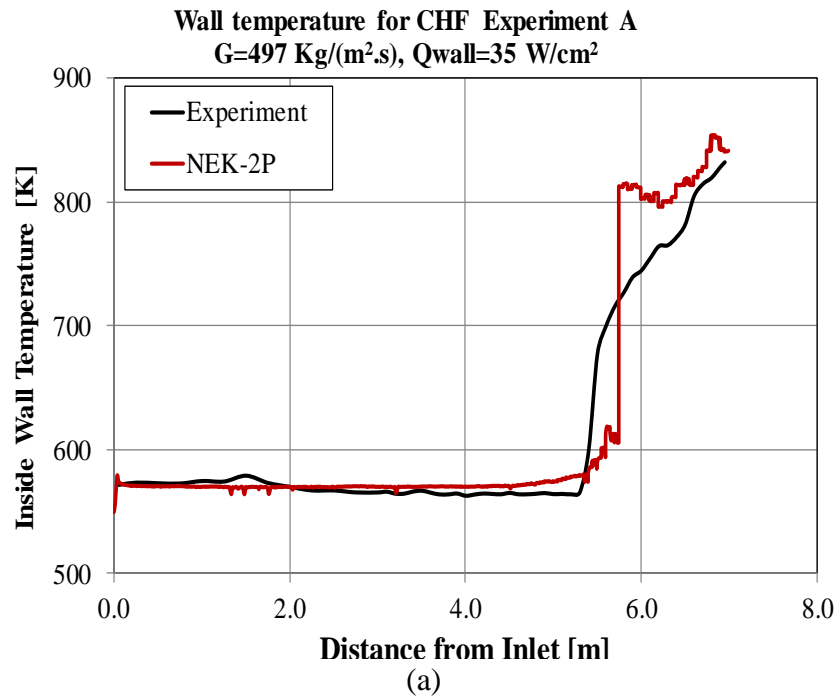
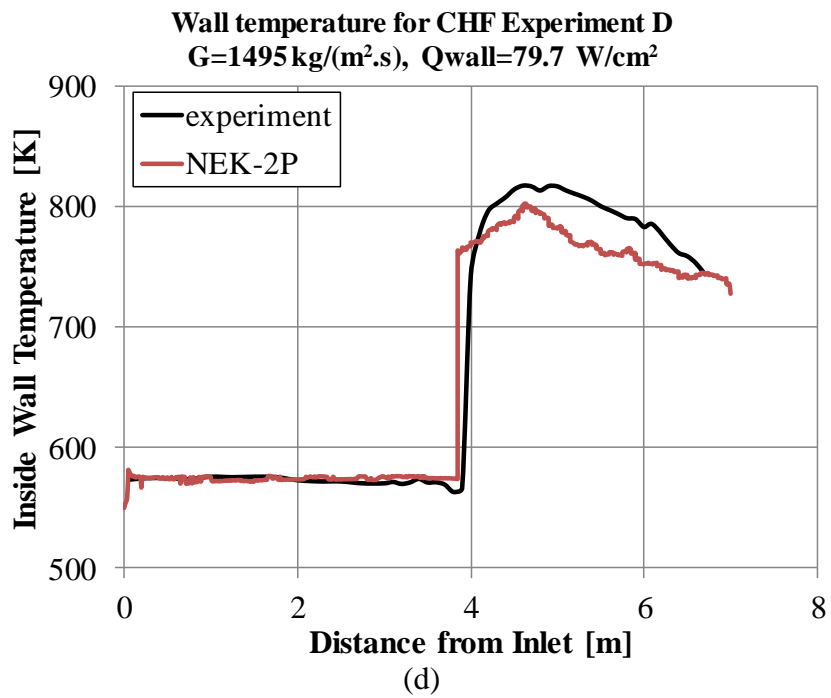
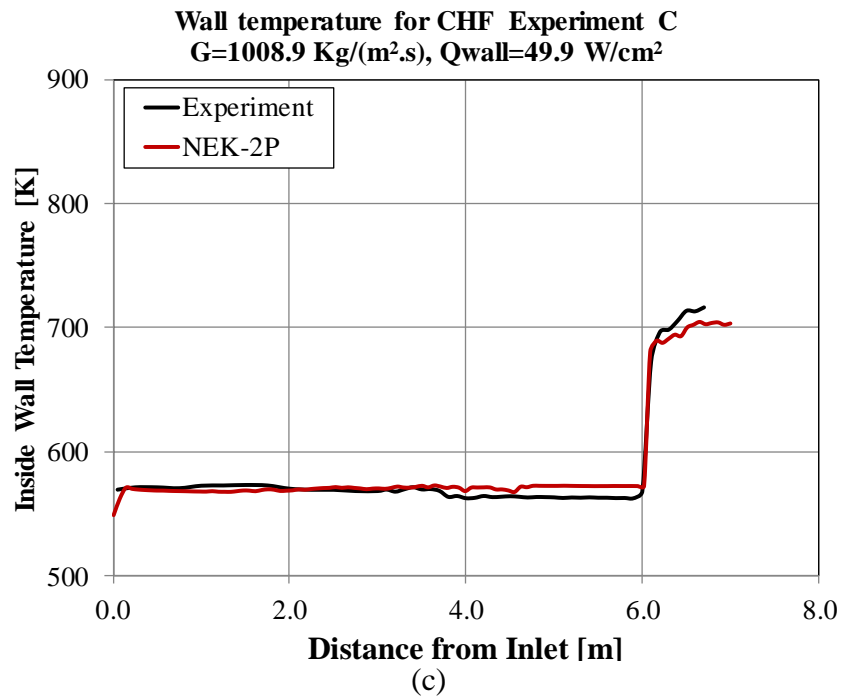


Figure 7. Vapor volume fraction along XZ-plane; (a) Experiment A, (b) Experiment B, (c) Experiment C, (d) Experiment D, (e) Experiment E and (f) Experiment F





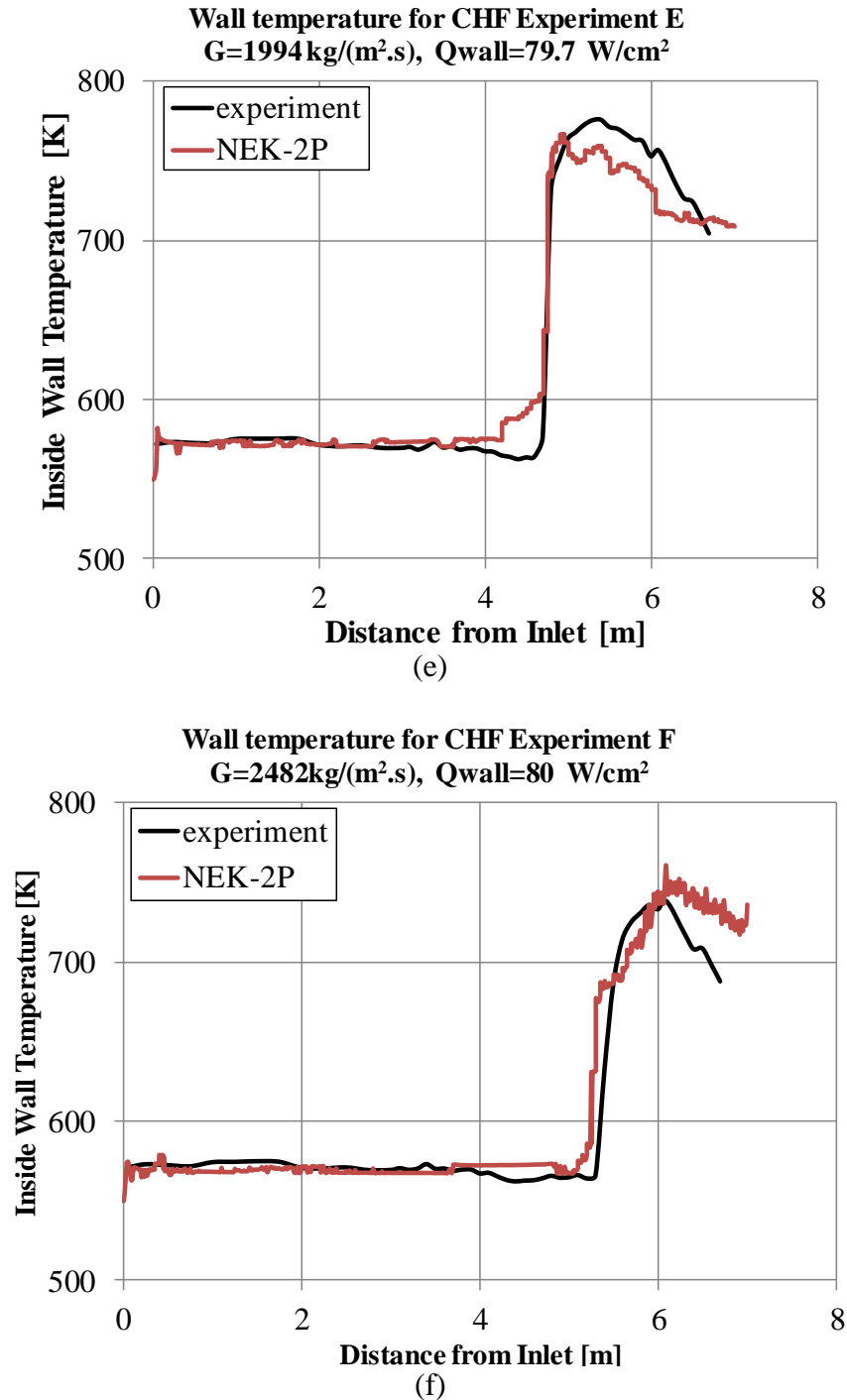


Figure 8. Wall temperature profiles along the tube height; (a) Experiment A, (b) Experiment B, (c) Experiment C, (d) Experiment D, (e) Experiment E and (f) Experiment F

The wall temperature calculated with the NEK-2P 2P-2F solver using the EBF from Tentner et al. [6] including the five-component wall partitioning model is compared with the corresponding

measured data. The location of the calculated sharp rise in the wall temperature agrees fairly well with the location of the measured wall temperature rise. The calculated sharp rise in the wall temperature coincides with the disappearance of the calculated liquid film on the pipe wall (Figure 7). Both the magnitude of the calculated wall temperature rise and the general shape of the wall temperature distribution in the post-dryout region are similar to the corresponding measured values.

For the experiments A and C the location of the calculated sharp rise in the wall temperature agrees reasonably well with the location of the measured wall temperature rise as shown in Figures 8a and 8c. In both cases the calculated sharp rise in the wall temperature coincides with the disappearance of the calculated liquid film (Figures 7a and 7c), indicating that there are few droplets at the dryout location and the liquid droplet entrainment does not play a significant role in these cases. The slope of the calculated wall temperature in the post-dryout region is similar to the corresponding measured temperature slope. The dryout location in experiments A and C moves further away from the pipe inlet as the ratio q_w/G - shown in Table 1 - decreases. For experiment B, which has a lower q_w/G ratio than experiment C (heat flux lower than C but a similar flow rate) the calculated wall temperature does not exhibit a sharp rise, in agreement with the measured temperatures indicating that film dryout did not occur in this case.

The dryout location in the experiments D-F, which were performed with the same wall heat flux, moves further away from the pipe inlet as the inlet coolant mass flux G increases and the ratio q_w/G - shown in Table 1 - decreases. The dryout location in experiment C, which had a lower wall heat flux and a lower coolant mass flux is the closest to the heated tube outlet, at approximately 6 m from inlet. The maximum post-dryout wall temperature for this experiment is substantially lower than the maximum wall temperatures observed for experiments D and E (Figure 8).

In the experiments D-F the calculated wall temperature peaks near the dryout location and decreases afterwards, in good agreement with the experimental temperature (Figures 8d and 8f). According to Hoyer [16], the wall temperature decrease in the post-dryout region is caused by evaporation of water droplets in superheated steam above the dryout elevation. This evaporation produces steam and therefore the vapor velocity increases rapidly. This in turn increases the wall-steam heat transfer coefficient and decreases wall temperature. This is consistent with the presence of droplets generated by film entrainment in the wall-cells at and above the dryout location, (Figures 7d-f). For experiment C, where the calculated amount of droplets in the wall-cells at the dryout location is low and the dryout location is close to the test section outlet, the post-dryout wall temperature decrease is not observed experimentally or in simulations (Figure 8c).

The NEK-2P results using the five component CHF DO wall heat transfer model described above in Section 2.5 capture the post-dryout wall temperature decrease better than the previous results due to the inclusion on the heat transfer between the water droplets and the heated wall. The vaporization of the water droplets in the near-wall cells in the post-dryout region is now driven both by the heat transfer between the superheated vapor and droplets and the heat transfer between the superheated wall and droplets providing an improved description of the CHF DO phenomena.

3.3 CONCLUSIONS

Results of NEK-2P analyses of Critical Heat Flux experiments conducted under DO conditions in a pipe with heated wall were presented. These analyses were performed using the NEK-2P two-phase two-fluid solver in conjunction with the Advanced Boiling Framework (ABF) closure models. The NEK-2P two-phase two-fluid model provides a satisfactory description of the vapor void fraction evolution expected in the CHF experiments and is able to capture the formation of liquid films on the heated pipe wall under DO conditions. The wall temperatures calculated by NEK-2P were compared with the corresponding experimental data. The calculated location of the CHF occurrence and the magnitude of the wall temperature increase closely match the corresponding experimental results. The distributions of the wall temperature downstream of the CHF location are also well predicted. Future work will focus on further development and validation of the NEK-2P CHF prediction models through additional analyses of boiling flow experiments relevant for Light Water Reactors (LWRs), including fuel-bundle two-phase flow experiments.

4 VALIDATION OF CHF DNB EXPERIMENTS

An attempt was made to develop standalone model to simulate Departure from Nucleate Boiling (DNB) phenomena in addition to the DO phenomena discussed above in Chapter 3. The developed model was used in preliminary simulations of DNB benchmark tests described in Section 4.1 below. Simulations of CHF experiments performed by Becker et al. [15] under DNB conditions.

4.1 SIMULATION OF TWO-PHASE BOILING FLOW IN CHF DNB EXPERIMENTS

The new six-component heat flux partitioning model described in Chapter 2 was used in preliminary simulations of the CHF DNB benchmark test G, H and I described above in Table 2. In these experiments the CHF occurs at a location where a significant amount of subcooled liquid is still present and the vapor remains concentrated near the heated wall. Results of simulations of experiment G using the five-component CHF DO model showed that the CHF DO model is not able to predict the CHF under DNB conditions. Results of NEK-2P simulations using the six-component DO-DNB heat flux partitioning model are shown in Figures. (9, 12, 14) and Figures. (10a, 13a, 15a) illustrating the calculated void fraction distribution and the wall temperature distribution, respectively. The calculated void fraction distribution shows a diminishing central region with subcooled liquid or near-zero void-fraction that extends to the pipe outlet and a growing vapor region near the heated pipe wall. This vapor distribution is markedly different from the distribution calculated with the same CHF DO-DNB model for the DO case E and shown in Figure 11b which shows the high void fraction central region and the thin liquid film formation typical for CHF DO cases. As shown in Figures. (9, 12, 14) the calculated DNB location and initial wall temperature increase agree well with the experimental data. The post-DNB wall temperature distribution agrees reasonably well with the observed temperatures. Future work will explore the effect of various ABF models on the post-DNB wall temperature behavior.

To explore the effect of the CHF DO-DNB model under DO and DNB conditions we analyzed the CHF DO experiment E and the CHF DNB experiment G with both the six-component DO-DNB model and the five-component DO model. Figure 11(a) shows that under DO conditions (experiment E) the wall temperatures predicted by the six-component DO-DNB model and the five-component DO model are relatively close and both agree reasonably well with the experimental data. However under DNB conditions (experiment G, Figure 9) the DO model is not able to predict the occurrence of DNB, while the DO-DNB model results are in good agreement with data.

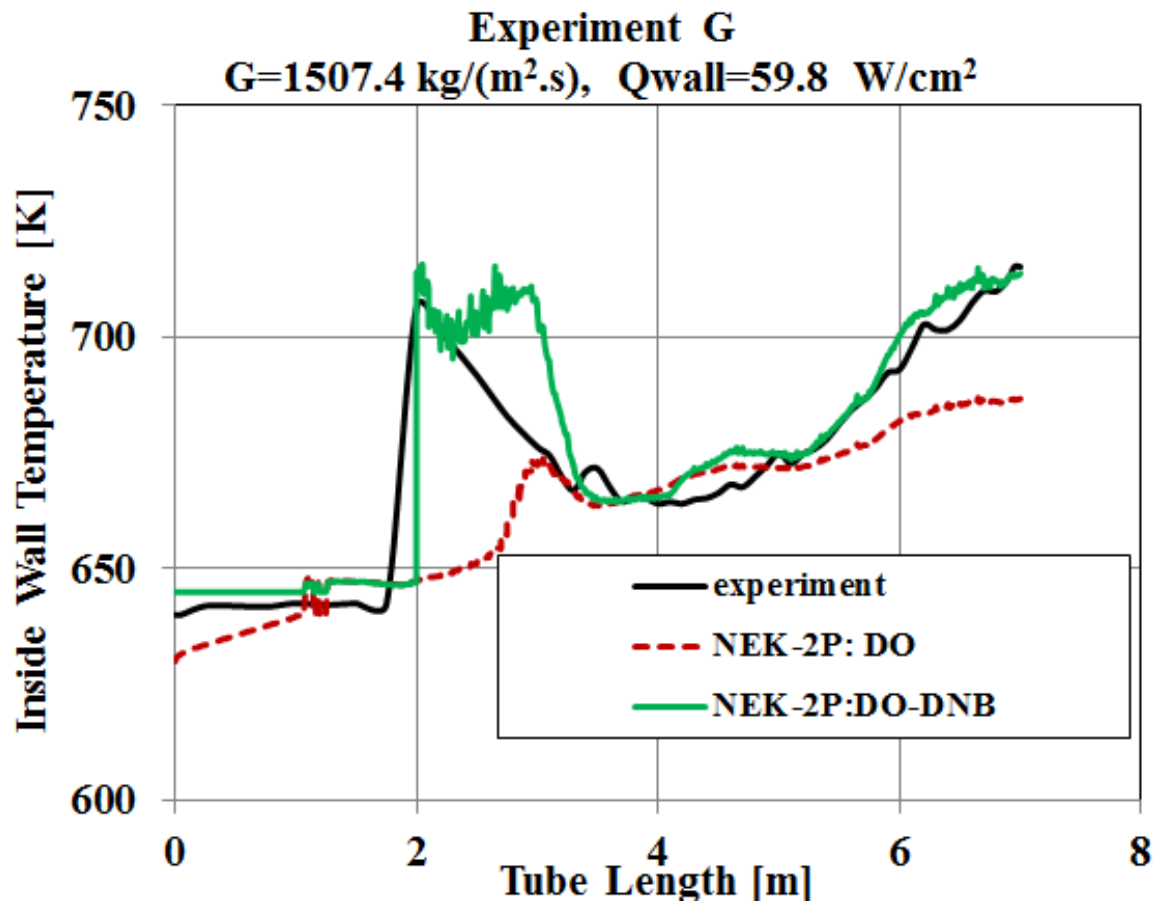


Figure 9. Wall temperature along the tube height for experiment G

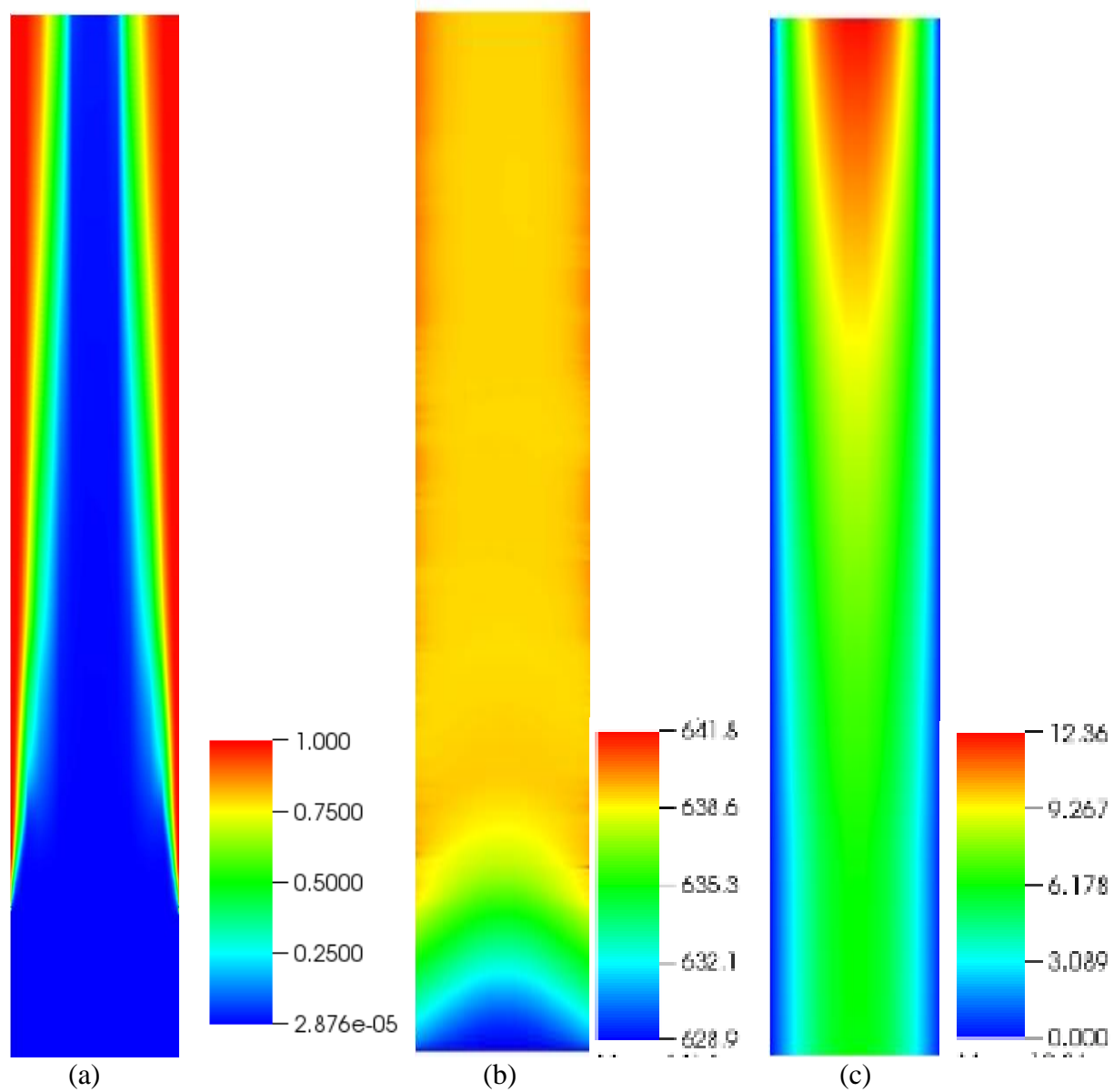


Figure 10. Contour fields for experiment G; (a) Vapor volume fraction, (b) Liquid temperature [K] and (c) Mixture velocity [m/s]

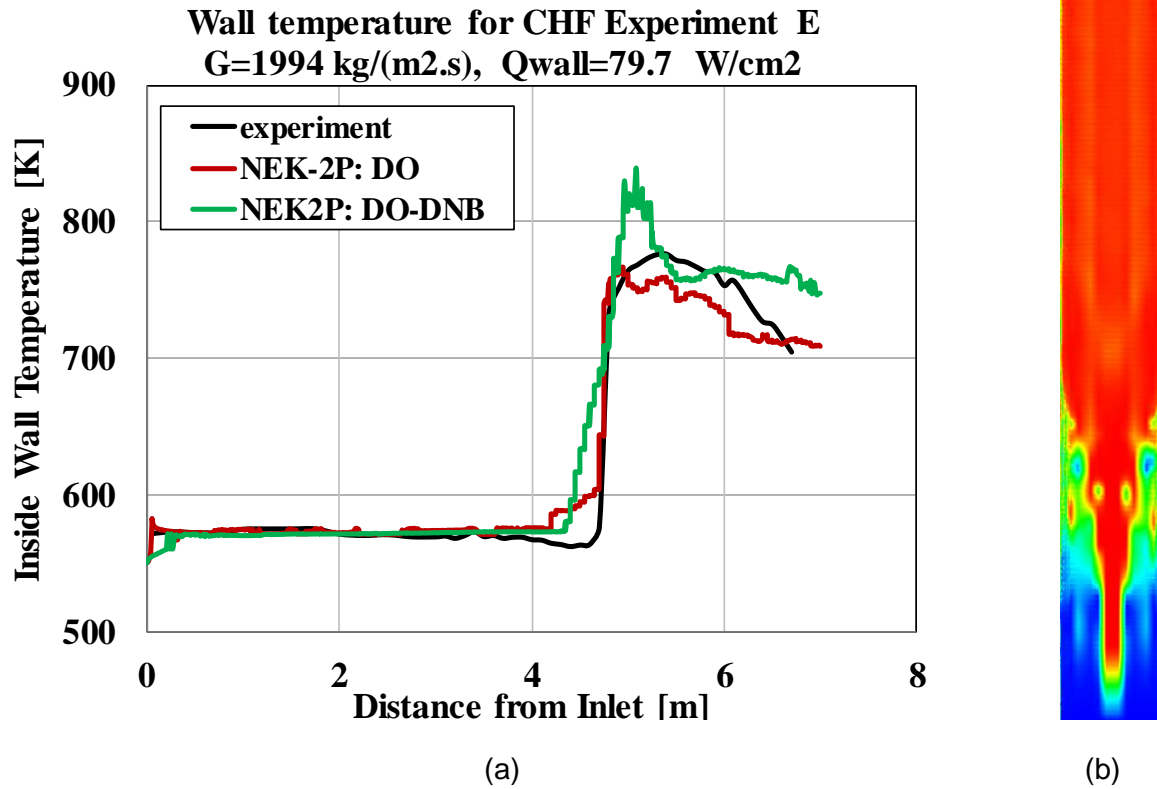


Figure 11. Comparison of NEK-2P DO and DO-DNB models; (a) Wall temperature along the tube length and (b) Vapor volume fraction on a vertical plane (XZ-direction)

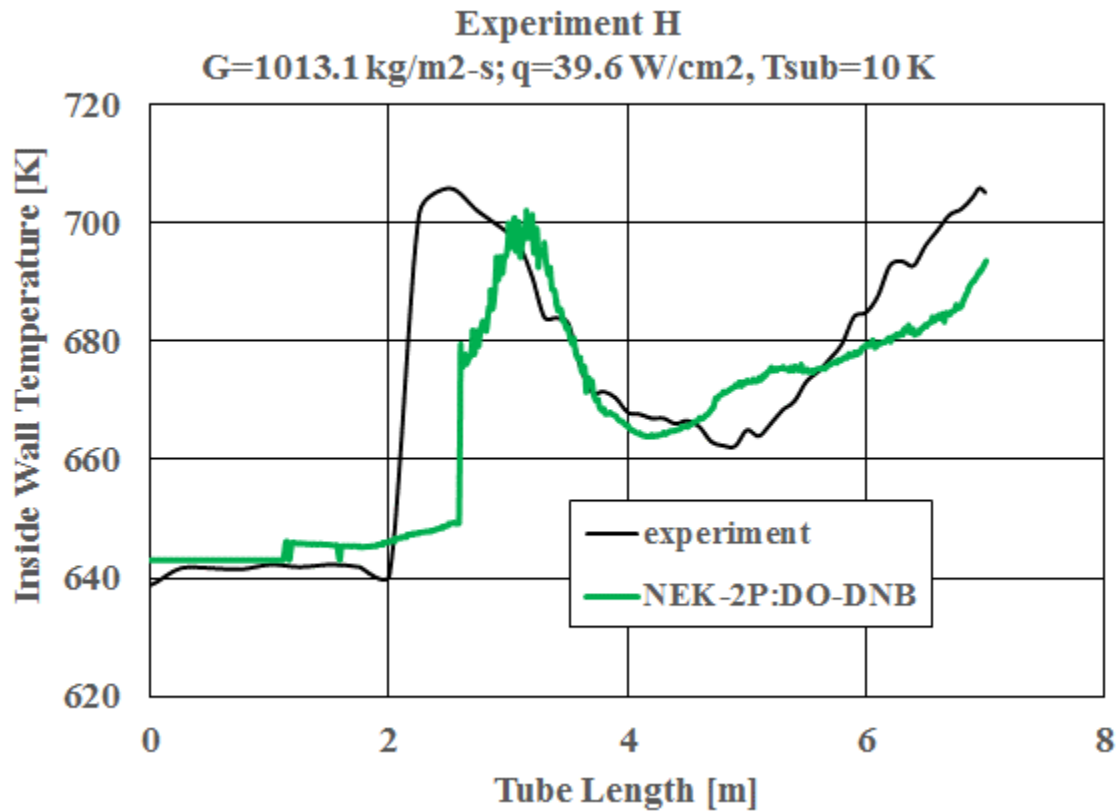


Figure 12. Wall temperature along the tube length for experiment H

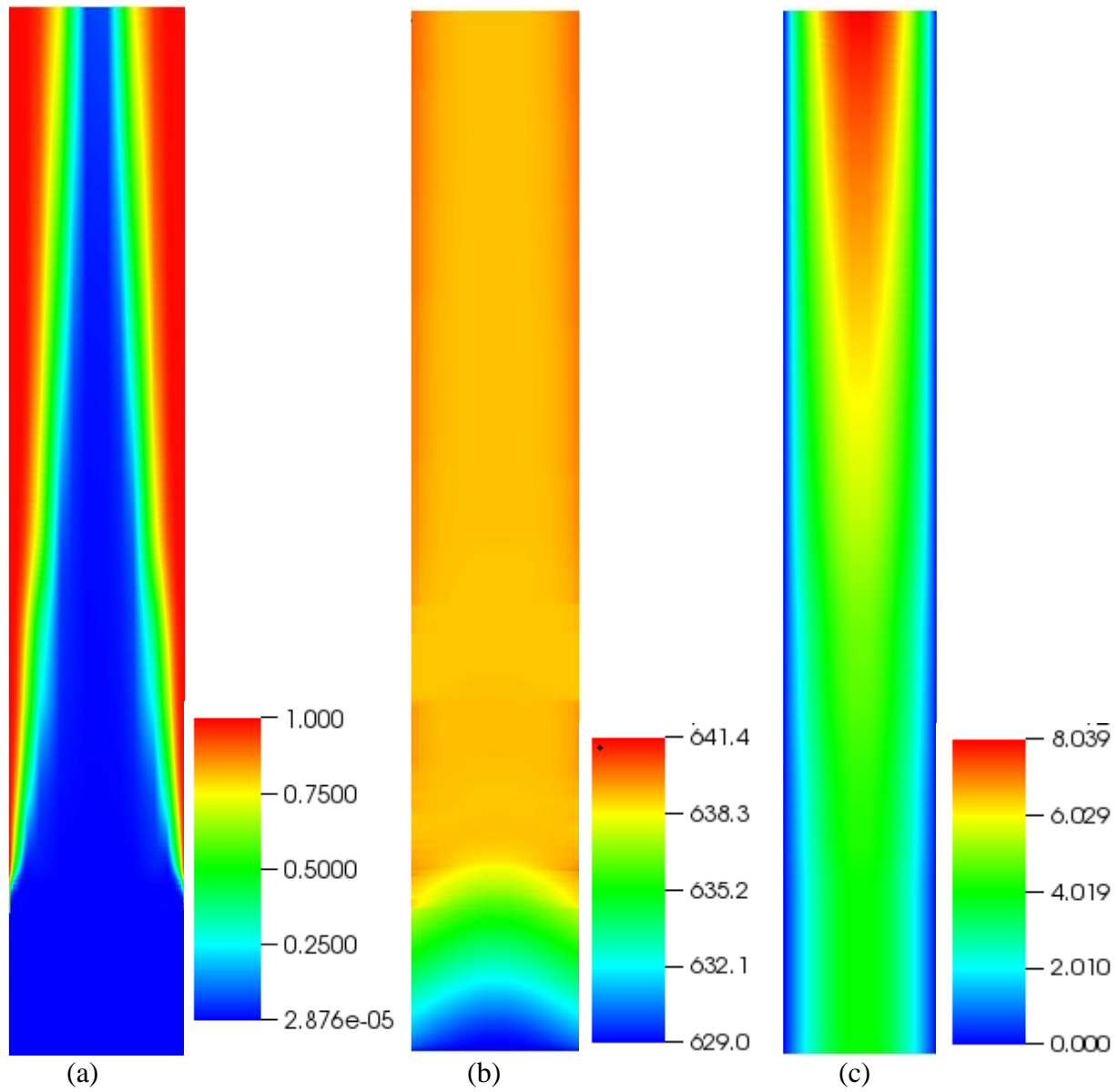


Figure 13. Contour fields for experiment H; (a) Vapor volume fraction, (b) Liquid temperature [K] and (c) Mixture velocity [m/s]

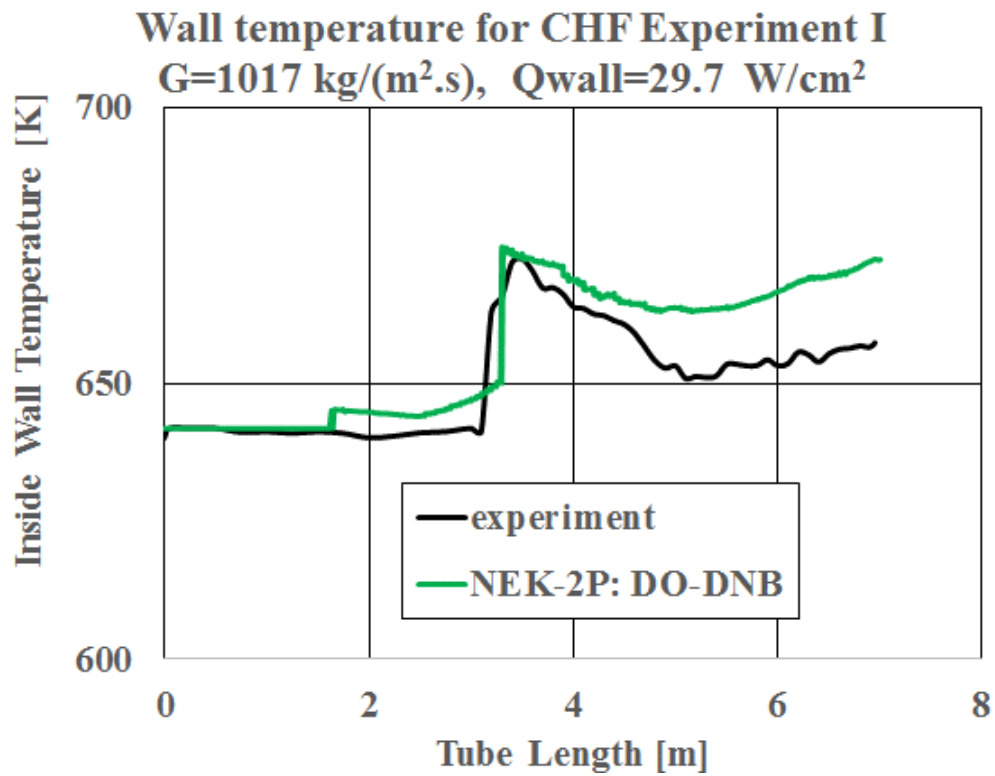


Figure 14. Wall temperature along the tube length for experiment I

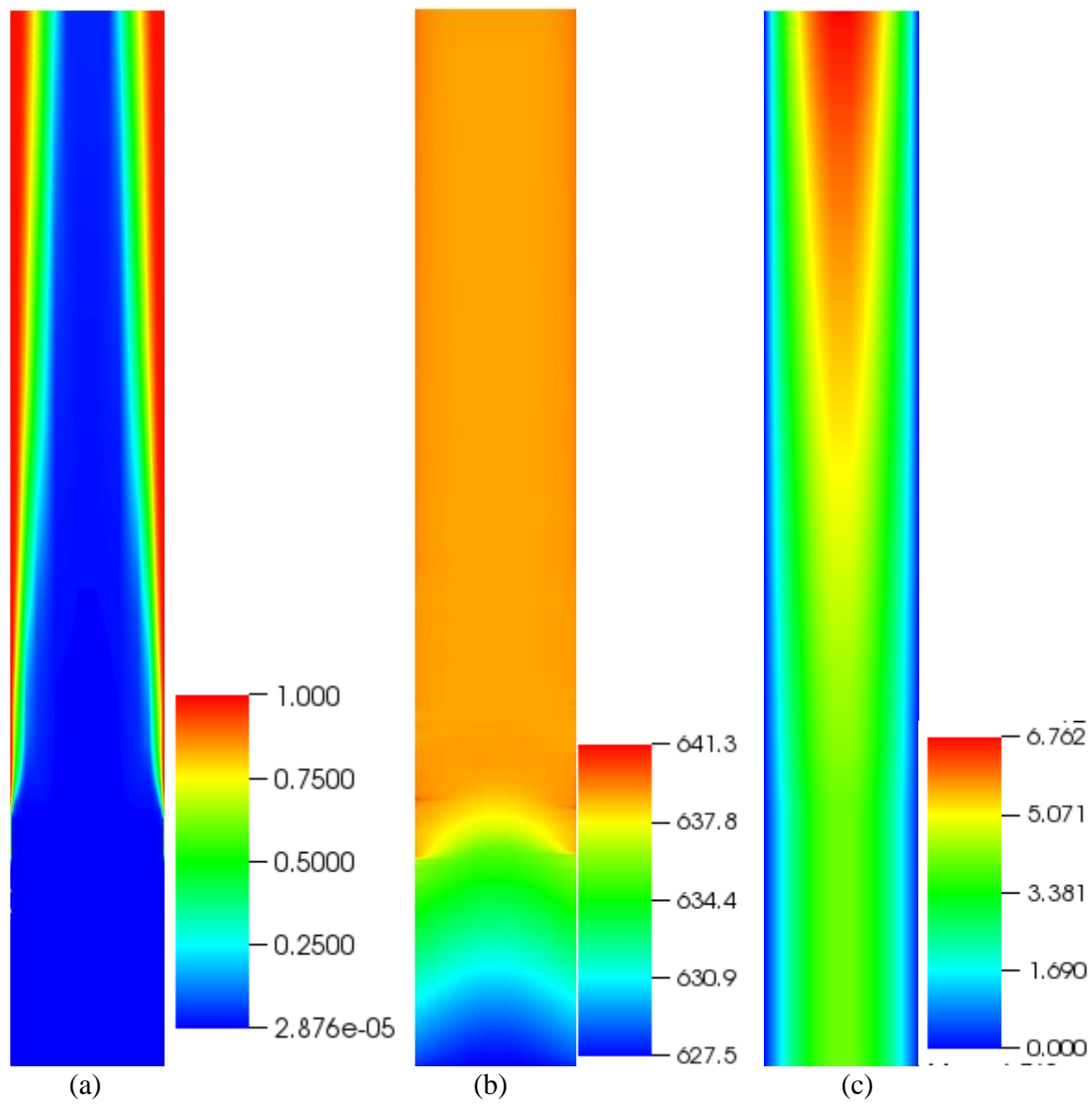


Figure 15. Contour fields for experiment I; (a) Vapor volume fraction, (b) Liquid temperature [K] and (c) Mixture velocity [m/s]

4.2 CONCLUSIONS

Results of NEK-2P analyses of Critical Heat Flux experiments conducted under DNB conditions in a pipe with heated wall were presented. These analyses were performed using the NEK-2P two-phase two-fluid solver in conjunction with the Advanced Boiling Framework (ABF) closure models. The NEK-2P two-phase two-fluid model provides a satisfactory description of the vapor void fraction evolution expected in the CHF experiments. The wall temperatures calculated by NEK-2P were compared with the corresponding experimental data. The newly developed DO-DNB wall heat transfer model predicts wall temperatures that are in reasonably good agreement with the wall temperatures measured under both CHF DO and CHF DNB conditions. In contrast, the DO model only valid for CHF DO experiments.

5 PRELIMINARY SIMULATIONS WITH CONJUGATE HEAT TRANSFER MODEL

5.1 CONJUGATE HEAT TRANSFER MODEL

An effort was initiated to develop a NEK-2P capability to simulate Conjugate Heat Transfer (CHT) phenomena in addition to DO and DO-DNB models, as discussed above. Preliminary simulations are underway for Becker benchmark test (experiment A) described in Section 3.1.1.

In this model, a NEKNEK script was used to run NEK-2P simulations for both fluid and solid domains. To be noted, the NEKNEK is a bash script and it executes two different Nek5000 simulations at a same time. The heat flux is specified at the outer surface of the vertical pipe, and the NEK-2P CHT model calculates the heat transfer through the pipe wall and heat transfer to the upward flowing fluid.

In the fluid domain, the NEK-2P solves liquid and vapor velocities, temperatures and mass fractions of both vapor and liquid. In the solid domain, the NEK-2P solves only for solid temperatures where the wall heat flux boundary condition applied to exterior of the solid surface. The heat flux at the solid-fluid interface processed as a source for the fluid domain and sink for the solid domain. The source and sink heat flux terms were calculated based on the fluid and the solid temperatures for a specified heat transfer coefficient. In FY19, the interface temperature will be updated using the wall heat flux-partitioning model.

Modeled boundary conditions at fluid-solid interface:

$$\text{Solid mesh: Sink} \quad [Q_s = -kSA \frac{dT}{dx}]$$

$$\text{Fluid mesh: Source} \quad [Q_L = \sum Q_i = -Q_s]$$

where, k_s is solid thermal conductivity and $\sum Q_i$ is sum of wall heat source components (see section 2.5)

In Figure 16, preliminary results are shown for vapor volume fraction and mixture velocity. Figure 17 shows the calculated solid and liquid temperatures. The evolution of the vapor volume fraction is in line with the liquid temperatures, where the liquid temperatures are greater than the saturation temperature. To be noted, the presented results are preliminary and yet to be converged.

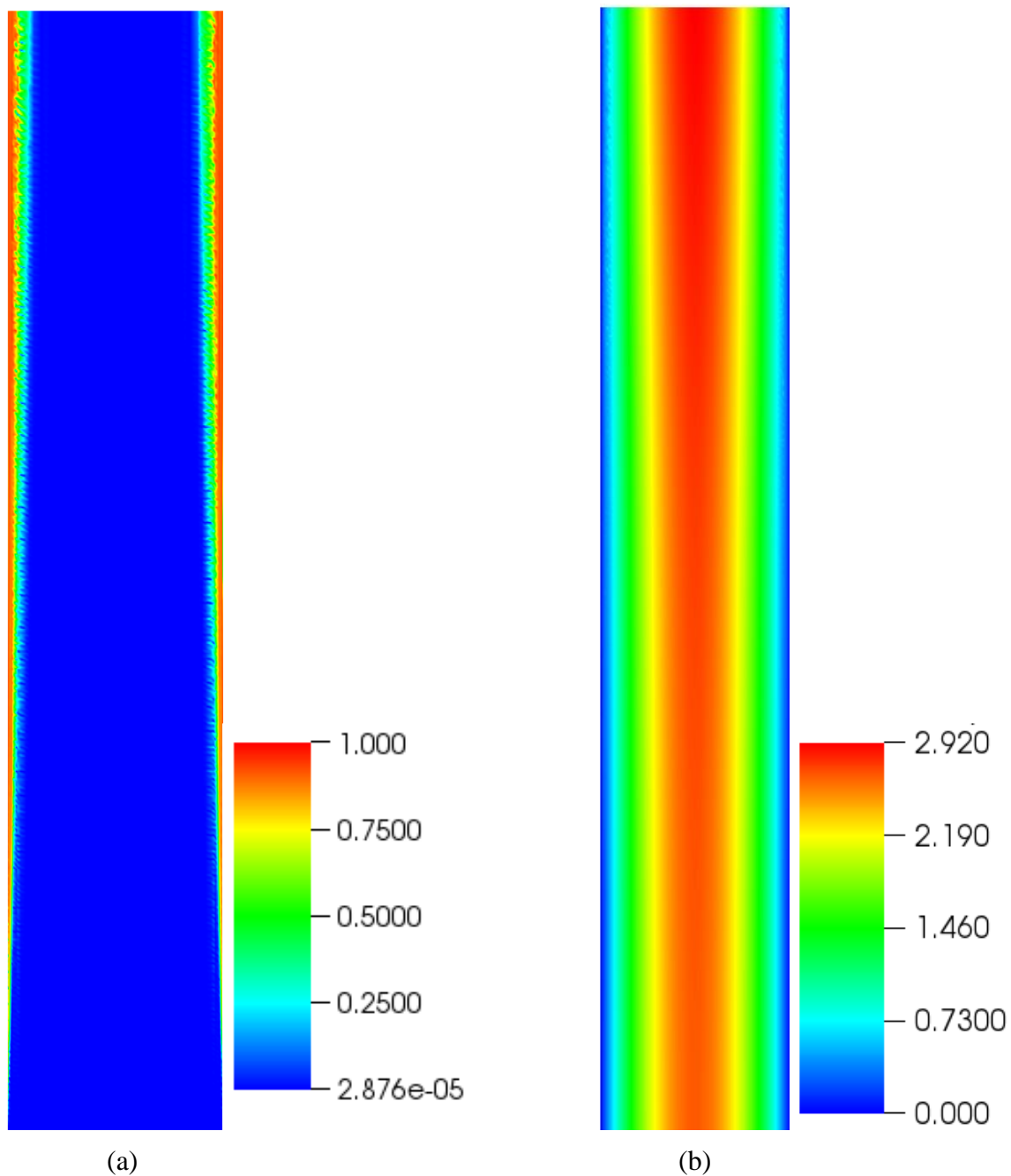


Figure 16. NEK-2P results along XZ-vertical slice for experiment A; (a) Vapor volume fraction and (b) Mixture velocity magnitude (m/s).

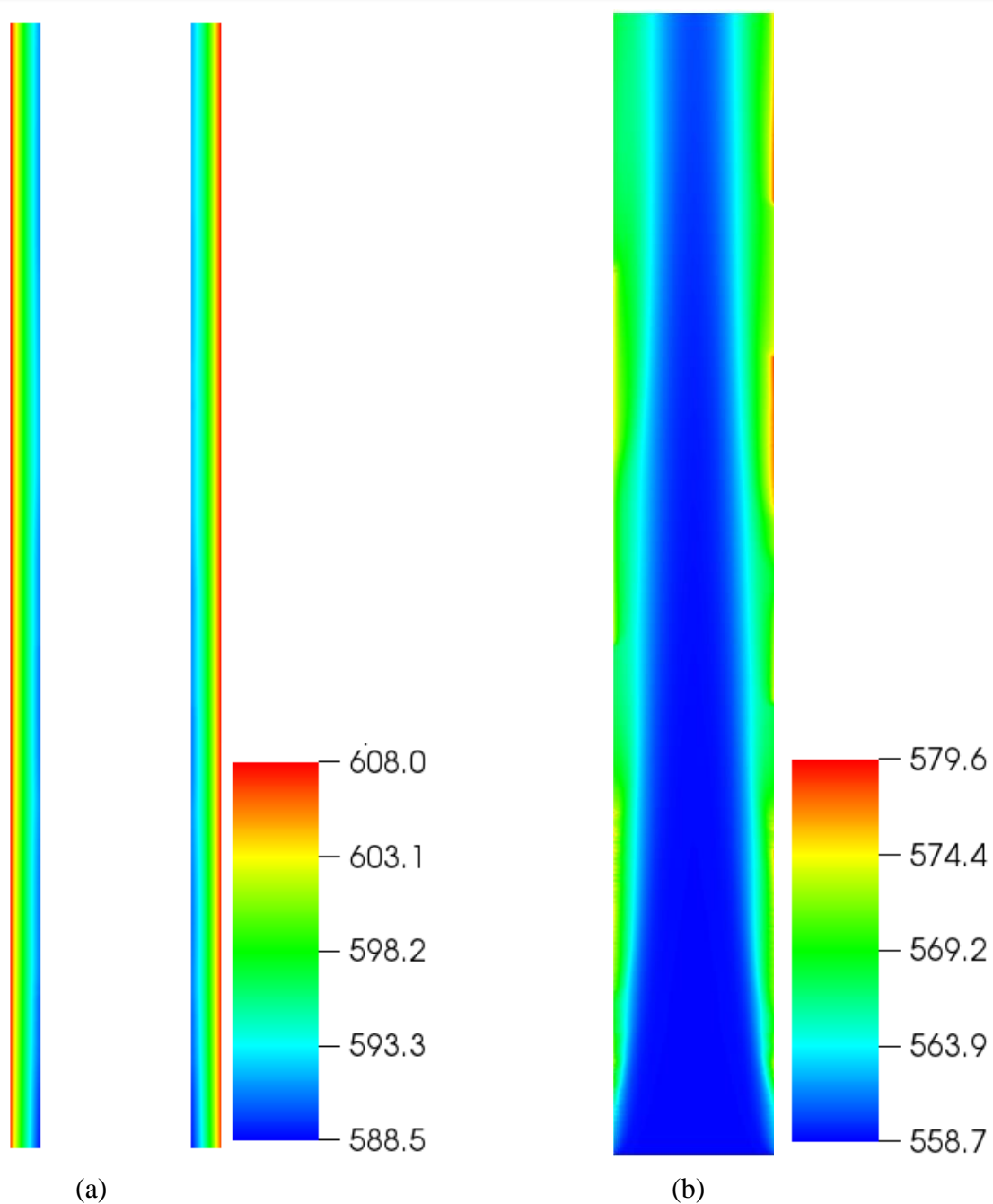


Figure 17. NEK-2P results along XZ-vertical slice for experiment A; (a) Solid temperature [K] and (b) Liquid temperature [K].

5.2 CONCLUSIONS

The initial conjugate heat transfer model was developed and implemented in NEK-2P. In this model, only the temperature equation is solved for the solid domain while phasic temperatures, velocities and mass fractions are solved in fluid domain. The heat flux source and sink terms are calculated at the interface of the fluid domain and the solid domain, respectively. The initial simulations are underway for one of the Becker DO experiments using the newly developed CHT model. In FY19, the interface boundary conditions will be updated to include the wall heat partitioning models.

6 SIMULATIONS OF AIR-WATER EXPERIMENTS

6.1 NEK-2P AIR-WATER SIMULATIONS

Air-Water experiments were conducted at Virginia Tech (VT) in the Air-Water Test Loop [17] as part of a Nuclear Energy University Program (NEUP) project that is focused on providing high resolution data for the validation of CFD Two-Phase Flow Codes. Preliminary NEK-2P simulations were performed in a vertical pipe with Diameter of 25.4 mm and Length of 3 m. In the test section, the measurements were taken at three axial locations and multiple radial locations as shown in Figure 18. As seen in Table 3, multiple experiments were performed at VT. Comparisons of the NEK-2P results with data are planned for FY2019 as the experimental report for the air-water experiments was only recently released.

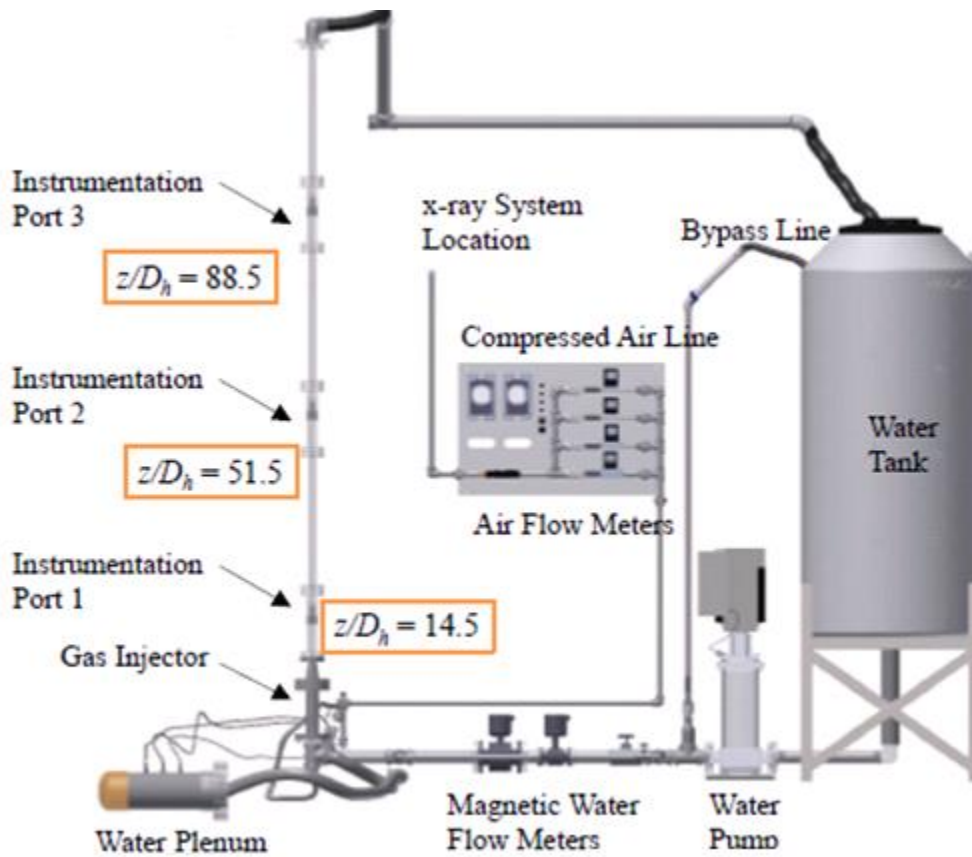


Figure 18. Schematic diagram for Air-Water reactor [17]

Table 3. Operating conditions for VT experiments [17]

Run #	1	2	3	4	5	6	7
j_f [m/s]	3.88	1.52	1.51	0.51	0.51	0.10	0.10
j_{g0} [m/s]	0.05	0.05	1.20	0.20	0.50	4.99	18.01

The schematic of the circular pipe test loop is shown in Figure 18. This facility is designed for adiabatic air-water two-phase flow at room temperature and near atmospheric pressure. In Table 3, j_{g0} and j_f are the superficial gas velocity and liquid velocity, respectively. These experiments were operated at 25 °C. In this report, initial simulations were performed for only Run 1.

In Figure 19, the calculated evolution of air distribution was shown at various axial locations. Near the inlet, a higher air void fraction was predicted in the annular region near the pipe wall than the core region void fraction ($Z/D_h=14.5$). Further downstream, the maximum air void fraction is predicted to occur in the core region. The contour plots for air distribution and mixture velocities predicted as expected in Figure 20. In FY19, multiple simulations are planned to validate the NEK-2P models with the data of VT measurements.

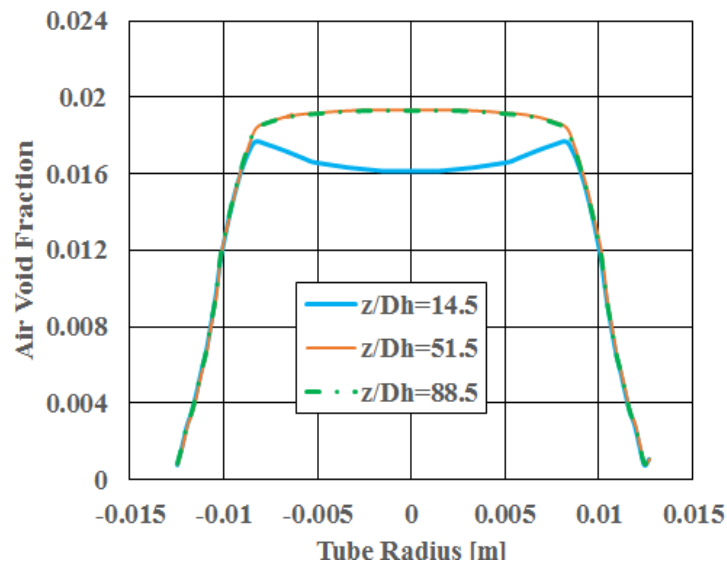


Figure 19. Air-water distribution at various axial locations for RUN-1 using $C_{lift}=0.02$.

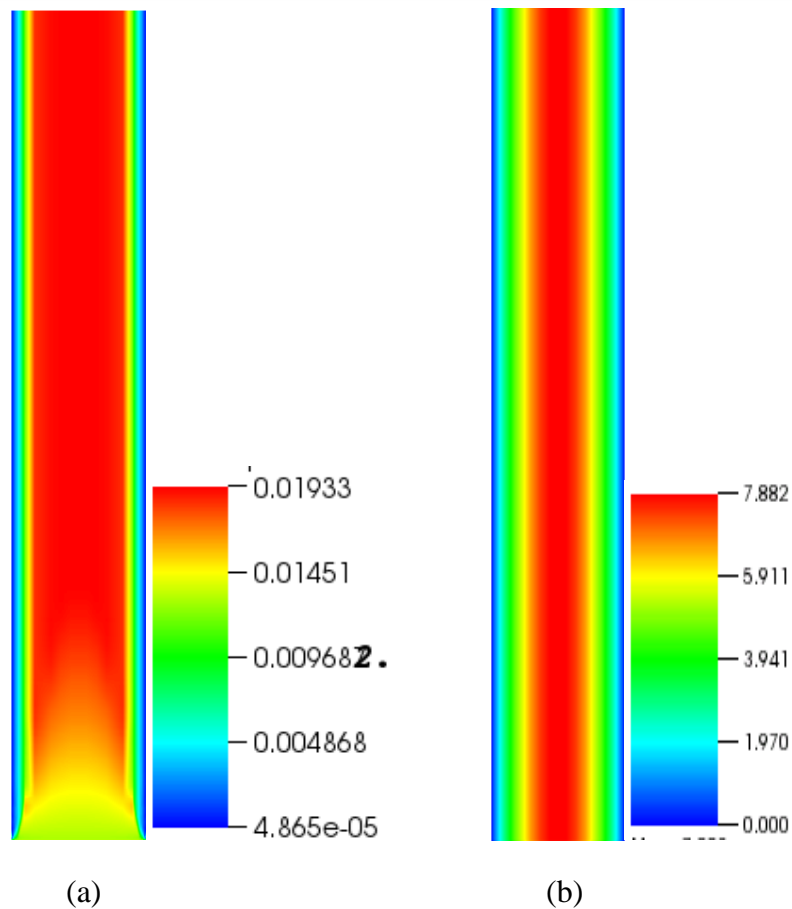


Figure 20. NEK-2P results along XZ-vertical slice of (a) Vapor volume fraction and (b) Mixture velocity magnitude (m/s).

6.2 CONCLUSIONS

Initial Air-Water simulations were performed using NEK-2P. In the inlet section, the maximum air void fraction was predicted in the annular region near the pipe wall. Further downstream, the maximum air void fraction was predicted in the core region. In future, the NEK-2P results will be validated with experimental data that was recently released by Virginia Tech (VT).

7 STATUS OF THE TWO-FLUID TWO-PHASE MODEL

The present work focuses on the development and initial validation of a two-phase two-fluid model (2F-2P) implemented in NEK-2P, including the prediction of CHF under both DO and DNB conditions. The NEK-2P two-phase two-fluid (2F-2P) solver is used to solve the continuity, momentum and energy equations for the vapor and the liquid phases.

A novel low Mach number numerical approach has been developed and implemented for the solution of the 2F-2P system of equations. In this approach, the pressure is assumed to be the same for both phases. The phase mass and energy equations are solved fully implicitly for the two mass fractions and temperatures, respectively, whereas the two-phase momentum equations are solved using a mixed explicit/implicit approach for the two phase velocities. The required phenomenological closures for the continuity, momentum and the energy equations were taken from the Extended Boiling Framework (EBF) work of Tentner et al. [2]. A new feature of the Advanced Boiling Framework (ABF) which is being implemented in the NEK-2P code is the use of a four-field two-phase generalized topology representation for a more accurate prediction of interfacial area and associated mass, momentum, and energy inter-phase transfer. The Critical Heat Flux prediction models have been extended to allow the simulation of CHF under both DO and DNB conditions. The extended CHF models were used successfully to predict the results of multiple CHF boiling experiments performed under DO and DNB conditions. Initial simulations of conjugate heat experiments were performed using newly developed NEK-2P conjugate heat transfer model.

8 FUTURE WORK

NEK-2P Development and Validation continues in FY2019 with a focus on CHF models enhancement and simulation of both DO and DNB experiments. Continue the collaboration with the NEUP project led by Virginia Tech (VT) and Michigan University (MU): (a) Continue analyses of water-air two-phase flow experiments began in FY2018, (b) Initiate analyses of heated bundle boiling experiments expected to begin at VT in FY2019 and (c) Continue the development of the NEK-2P conjugate heat transfer capability and its validation. We also plan to initiate the collaboration with the CASL program focused on the NEK-2P analysis of selected two-phase water-air experiments and comparison with STAR-CCM+ results.

ACKNOWLEDGMENTS

This work was funded by the U.S Department of Energy, Office of Nuclear Energy, Nuclear Energy Advanced Modeling and Simulation (NEAMS) program, under Argonne contract DE-AC02-06CH11357.

We gratefully acknowledge the computing resources provided on Bebop, a high-performance computing cluster operated by the Laboratory Computing Resource Center at Argonne National Laboratory.

9 REFERENCES

1. Fischer et al., Petascale algorithms for reactor hydrodynamics, J. Phys. Conf. Series (2008)
2. Tentner et al., Computational Fluid Dynamics Modeling of Two-phase Flow in a Boiling Water Reactor Fuel Assembly, Proc. Intl. Conf. Mathematics and Computations, American Nuclear Society, Avignon, France, Sept. 2005.
3. Tentner et al., Integral Validation of a CFD Model for the Simulation of Two-Phase Flow Phenomena in a Boiling Water Reactor: Analyses of the BFBT Full Bundle Tests, Nuclear Engineering and Design, June 2009
4. Ustinenko et al., Validation of CFD-BWR, a new two-phase computational fluid dynamics model for boiling water reactor analysis, Nuclear Engineering and design 238 (2008) 660-670.
5. Tentner et al., Computational fluid dynamics modeling of two-phase boiling flow and critical heat flux, Proc. Intl. Conference on Nuclear Energy ICONE-22, Prague, 2014.
6. Tentner et al., Modeling of Two-Phase Boiling Flow and Critical Heat Flux with the NEK-2P CFD Code, Proc. Intl. Conference on Nuclear Energy ICONE-25, Shanghai, 2017.
7. Tentner et al., Modeling of two-phase flow in a BWR fuel assembly with a high-fidelity CFD code, NURETH-16, Chicago, 2015.
8. Tentner et al. Advances in computational fluid dynamics modeling of two phase flow in a boiling water reactor fuel assembly”, Proc. Int. Conf. Nuclear Engineering ICONE-14, Miami, Florida, USA, July 17-20, 2006.
9. Tentner et al. Development and Validation of an Extended Two-Phase CFD Model for the analysis of Boiling Flow in Reactor Fuel Assemblies”, Proc. Int. Conf. Advances in Nuclear Power Plants, Nice, France, May 13-18, 2007.
10. Tomboulides and Orszag, A quasi two-dimensional benchmark problem for low Mach number compressible codes, Journal of Computational Physics, 146, p.691-706, 1998.
11. Tomboulides et al., Numerical simulation of low Mach number reactive flows, Journal of Scientific Computing, 12(2), p.139-167, 1997.
12. Tentner et al. Computational Fluid Dynamics Modeling of Two-Phase Flow and Inter-Phase Surface Topologies in a BWR Fuel Assembly,” Proceedings of ICONE16, the 16th International Conference on Nuclear Engineering, Orlando, FL, USA, May 11-15, 2008.
13. Kurul N., Podowski, M., “Multidimensional effects in sub-cooled boiling”, Proc. 9th Heat Transfer Conference, Jerusalem (1990).
14. Tentner, A., Vegendla, P., Tomboulides, A., Obabko, A., Merzari, E., Shaver, D. Advances in Modeling Critical Heat Flux in LWR Boiling Flows with the NEK-2P CFD Code. 26th int. conf. on Nuclear Engineering (ICONE 26), 2018.
15. Becker et al., An experimental investigation of post-dryout heat transfer, Department of Nuclear Reactor Engineering, Royal Institute of Technology, KTH-NEL-33, Sweden, 1983.

16. Hoyer N., Calculation of dryout and post-dryout heat transfer for tube geometry. *Int. J. Multiphase Flow*, 1998, Vol.24, No.2, p. 316-334.
17. Wang et al. Data Report on Two-Phase Flow Measurements in a 25.4 mm Round Pipe Facility. 2018, NEUP, DOE, VT/MFTL-18-01.



Nuclear Science and Engineering Division

Argonne National Laboratory
9700 South Cass Avenue, Bldg. 208
Argonne, IL 60439

www.anl.gov



**U.S. DEPARTMENT OF
ENERGY**

Argonne National Laboratory is a U.S. Department of Energy
laboratory managed by UChicago Argonne, LLC